

DESIGN AND MANUFACTURING OF VARIABLE STIFFNESS CELLULAR  
ARCHITECTURE

A Thesis  
Submitted to the Graduate Faculty  
of the  
North Dakota State University  
of Agriculture and Applied Science

By  
Ruinan Xie

In Partial Fulfillment of the Requirements  
for the Degree of  
MASTER OF SCIENCE

Major Department:  
Industrial and Manufacturing Engineering

November 2017

Fargo, North Dakota

North Dakota State University  
Graduate School

---

**Title**

Design and Manufacturing of Variable Stiffness Cellular Architecture

**By**

Ruinan Xie

The Supervisory Committee certifies that this *disquisition* complies with North Dakota State University's regulations and meets the accepted standards for the degree of

**MASTER OF SCIENCE**

SUPERVISORY COMMITTEE:

Dr. Bashir Khoda

Chair

Dr. Om Prakash Yadav

Dr. Chad Ulven

---

Approved:

11/17/2017

Date

Dr. Om Prakash Yadav

Department Chair

## **ABSTRACT**

Cellular structures are highly evaluated due to their high material efficiency. Both theoretical and experimental studies have done on periodic cellular structures. However, the mechanical performance can be stochastically distributed in the cellular architecture. This thesis presents the design and manufacturing of variable stiffness cellular architecture to achieve optimized topology by changing the unit cell parameters. The author applies image analysis technique to extract and digitize the information from the performance distribution map. Two types of cellular cells are studied for their relationship of stiffness and relative density. The methods of voxelization for both cells are also given in this study. This proposed methodology is then implemented to design a customized mattress and compare with current existing mattress. With the study of the unit cells and voxelization technique, our designed mattress aligns body curve better which provides more recuperation of the body during sleep.

## **ACKNOWLEDGEMENTS**

I give my deepest gratitude to my advisor, Dr. Bashir Khoda, for the guidance and support throughout my whole graduate education. Thank him for the unmeasurable help in this research with his knowledge and expertise on advanced manufacturing.

I would also like to acknowledge my committee members, Dr. Yadav and Dr. Ulven for their help and valuable advice with this research.

My appreciation also extends to my lab colleague, AMM Nazmul Ahsan and MD Ahasan Habib who sustain a positive study atmosphere and shared their experience to help me avoid many detours in study and research.

Finally, I would say thanks to my family members and friends for their financial and mental supports. I can't finish the degree without their constant encouragement and love.

## TABLE OF CONTENTS

ABSTRACT .....	iii
ACKNOWLEDGEMENTS .....	iv
LIST OF TABLES .....	vii
LIST OF FIGURES .....	viii
LIST OF SYMBOLS .....	xi
1. INTRODUCTION .....	1
1.1. Significance of the Work.....	2
1.2. Objective of Research .....	3
1.3. Overview of Research .....	3
2. LITERATURE REVIEW .....	5
2.1. Cellular Structure .....	5
2.1.1. Closed Cell .....	6
2.1.2. Open Cell.....	7
2.2. Fabrication Methods of Cellular Structure.....	8
2.2.1. Closed Cell Fabrication .....	8
2.2.2. Open Cell Fabrication.....	11
3. TOPOLOGY DESIGN FOR CLOSED CELL.....	13
3.1. Image Performance Data Extraction .....	13
3.2. Relationship between Unit Honeycomb Cell Performance and Parameter.....	15
3.2.1. Gibson-Ashby Model of Cellular Structure Deformation .....	15
3.2.2. Structure Characterization and Selection of Parameters for Regular Hexagonal Honeycomb .....	16
3.2.3. Study on Unit Cell Parameter.....	17
3.3. Voxelization .....	24

3.4. Fitting Unit Cell .....	26
4. TOPOLOGY DESIGN FOR OPEN CELL .....	28
4.1. Relationship between Unit Cuboid Cell Performance and Parameter .....	28
4.1.1. Structure Characterization and Selection of Parameters .....	28
4.1.2. Study on Unit Cell Parameter.....	30
4.2. Voxelization .....	35
4.3. Fitting Unit Cell .....	38
5. IMPLEMENTATION.....	39
5.1. Method Validation: Customized Mattress.....	39
5.2. Evaluation.....	43
6. CONCLUSION AND FUTURE DIRECTION .....	46
6.1. Conclusion.....	46
6.2. Future Direction .....	46
REFERENCES .....	48

## LIST OF TABLES

<u>Table</u>	<u>Page</u>
1. Periodic Honeycomb Structures with Different Cell Types .....	7
2. Design of Experiment of Regular Hexagonal Honeycombs.....	18
3. Young's Modulus of All Silicone Hexagon Specimens .....	23
4. Analysis of Six Types of Unit Cells and Their Relative Density .....	29
5. Design of Experiment of Cuboid .....	30
6. Young's Modulus of Wire Structures .....	34

## LIST OF FIGURES

<u>Figure</u>	<u>Page</u>
1. Examples of cellular material (A-M Harte, Fleck, & Ashby, 1999): (a) closed cell alporas foam and (b) open cell duocel foam.....	5
2. Examples of three types of honeycomb as core in sandwich structures (Wadley, 2006): (a) hexagonal honeycomb, (b) square honeycomb and (c) triangular honeycomb.....	6
3. Schematic drawings of six type unit open cells in cellular structure (Ahmadi et al., 2015): (a) cubic; (b) diamond; (c) truncated cube; (d) truncated cuboctahedron; (e) rhombic dodecahedron; (f) rhombicuboctahedron .....	8
4. Illustration of expended honeycomb manufacturing process (Wadley, 2006) .....	9
5. Illustration of corrugation manufacturing process (Wadley, 2006).....	10
6. Illustration of strip slotting method (Wadley, 2006) for making (a) square honeycomb and (b) triangular honeycomb.....	10
7. Illustration for the manufacturing method of pyramidal cores (Kooistra & Wadley, 2007) .....	11
8. Wire lay-up process (Wadley, 2006) (a) layup wire, (b) core wires bonded and cut .....	12
9. Cellular structure with AM (a) CAD model of cellular structure, (b) failed sample (Bauer et al., 2014).....	12
10. Flow diagram of proposed methodology .....	13
11. (a) Image with heterogeneous porosity, (b) corresponding quantized images with $l = 8$ .....	15
12. Hexagon parameters.....	17
13. Compression load applied on hexagonal honeycombs along Z direction.....	18
14. CAD file of the test samples with change on thickness (unit: mm).....	19
15. Specimen casting process: (a) the designed CAD model of mold, (b) mold printing with Makerbot z18, (c) pouring silicone with syringe into the mold, (d) demold the cast after curing for 4 hours .....	20
16. Compression test applied on silicone hexagonal structure (a) no load applied; (b) applying load to the structure; (c) 50% deformation happened to the structure .....	21
17. Compression test result of all specimens with different thickness, (a) $t = 2$ , (b) $t = 3$ , (c) $t = 4$ and (d) $t = 5$ (unit: mm).....	21



18. Failure mode for different thickness, (a) 2mm, (b) 3mm, (c) 4mm, (d) 5mm .....	22
19. Plot of the Young's Modulus vs relative density for silicone hexagonal samples .....	24
20. Voxel size parameters .....	25
21. Hexagon unit cell fitting into voxel, (a) an example of voxelization result, (b) hexagon outlines are drawn with the equation, (c) the real honeycomb structure with variation thickness.....	27
22. Cuboid parameters .....	28
23. (a) CAD model of $5 \times 5 \times 1$ structure, (b) study of each single unit cell and their cell type ....	29
24. Wire bending process of making cuboid structures .....	31
25. (a) Structure after bend, (b) structure after surface treatment, (c) structure after epoxy bonded .....	31
26. Compression test applied on wire structure (a) structure before apply load, (b) 80% deformation happened.....	32
27. Compression test results of all specimens with $l = h = 10$ , where (a) $w = 8$ ; (b) $w = 10$ ; (c) $w = 12$ and (d) $w = 14$ (unit: mm).....	33
28. Failure modes of Cuboid Structure, (a) fan-spread buckling, (b) sway buckling.....	33
29. Young's Modulus vs relative density plot for wire structures. ....	34
30. Cuboid voxel parameters .....	35
31. Parametric functions generated for the example image .....	37
32. Example of voxelization .....	38
33. Cuboid unit cell fitted into voxels, (a) top view of an example of voxelization, (b) cells fitted into the 3d voxels, (c) CAD model of the variable sized cuboid cellular structure. ....	38
34. Load distribution map on mattress ("Pressure Imaging for Mattress Design," 2013) .....	39
35. Quantized image, respectively at $l = 32$ .....	40
36. Body postures.....	41
37. Idea body curvature.....	41
38. Voxelization of the proposed design of mattress .....	42

39. Fitting variable hexagons into voxels .....	43
40. Model of uniform hexagonal mattress .....	44
41. Comparison of the deformation between two designs .....	44

## LIST OF SYMBOLS

$\rho^*$	.....	Density of the cellular structure
$\rho_s$	.....	Density of the material constituting the cellular structure
$E^*$	.....	Young's Modulus of the cellular structure
$E_s$	.....	Young's Modulus of the material constituting the cellular structure
$\sigma$	.....	Stress of the cellular structure
$\varepsilon$	.....	Strain of the cellular structure
$F$	.....	Load applied on the cellular structure
$A$	.....	Surface area of the cellular structure
$t$	.....	Wall thickness of the hexagonal honeycomb
$l$	.....	Cellular unit cell length
$w$	.....	Cellular unit cell width
$h$	.....	Cellular unit cell height
$\Delta h$	.....	Deformation of cellular unit cell in Z direction
$D$	.....	Wire diameter for wire cellular structure

## 1. INTRODUCTION

Cellular materials are those materials that introducing substantial porosity to a solid material where the effective properties can be obtained (Maloney et al., 2013). With the inspiration of these natural materials, people started design and manufacturing cellular structures and applied into many industries including aerospace (Evans, Hutchinson, Fleck, Ashby, & Wadley, 2001), biomedical (Ahsan, Xie, & Khoda, 2017; Hollister, 2005), and building construction (Nonell, 2000; Shipbuilding), etc.

Periodic cellular metals are most known man made cellular structure which widely used in the design of light weight sandwich panel structures for energy absorption (Banhart, 2001; Anne-Marie Harte, Fleck, & Ashby, 2000; Jian Xiong, Ma, Wu, Wang, & Vaziri, 2010) and heat transfer (Bitzer, 2012; Lu & Chen, 1999). Extensive studies have performed on hexagonal honeycombs and proved that the mechanical properties has a proportional relationship to its relative density. People provides different fabrication processes to make these periodical cellular structures, e.g., corrugation process, strip slot methods, casting and foaming (Deshpande & Fleck, 2001; Kooistra & Wadley, 2007; Wadley, 2006; Zok et al., 2004).

Similar studies also extend to those opened cellular cells including pyramidal truss structure (Chen, Zhu, Lei, Chen, & Fang, 2015; George, Deshpande, & Wadley, 2013; J Xiong et al., 2012), octec-truss structure (Dong, Deshpande, & Wadley, 2015; Dong & Wadley, 2016), Kagome structure (HL Fan, Meng, & Yang, 2007; Hualin Fan, Yang, Sun, & Fang, 2013) and corrugated lattice truss structure (Hu, Li, An, & Fan, 2016). These 3D cellular structures are looked as the most weight-efficient structure (Jiang, Sun, Zhang, & Fan, 2017). Changing the truss diameter or cell parameters will cause the change of relative density and the mechanical performance. Approaches of fabricate these types of structure will be more complicate including

perforated method and wire lay-up process (Wadley, 2006). But these traditional methods will have difficulties when making complex cell geometry. Here additive manufacturing technology can be applied for fabrication of complex cells with certain material. Electron-beam melting (EBM) and selective laser melting are suitable for this task (I. Gibson, Rosen, & Stucker, 2010; Kruth, Leu, & Nakagawa, 1998).

Most researchers focused on the periodic cellular structures (Grediac, 1993; Kelsey, Gellatly, & Clark, 1958; Maskery et al., 2017; Triantafyllidis & Schraad, 1998) which will maintain the mechanical property periodically. However, the performance or mechanical property required in an object can be stochastic. In this case, the study of the variable performance cellular structure becomes necessary. This thesis proposed a method of design and fabrication process of variable stiffness cellular structure by focus on the stochastic performance of the object.

### **1.1. Significance of the Work**

Periodic cellular structures are studied and applied in many disciplines due to its high material efficiency and strength to material ratio. Actually, the material efficiency of the cellular structure can be enhanced by doing topology design of variable performance cellular structure. Ajdari studied the functional graded cellular structures and its energy absorption performance (Ajdari, Nayeb-Hashemi, & Vaziri, 2011). The results shows that introduce the density gradient will significantly improve the performance.

However, the performance can be stochastically distributed along the structure, so the study of the performance distribution is very important, here in this work, an image analysis technique is applied to quantize the performance distribution in pixel-sized level. And two methods of voxelization is introduced after find the relationship between the performance and cell size. And as the variation density cells appeared in the design, difficulties encounter to fabrication process.

A new wire bending methods to fabricate variable density metal cellular structure is introduced here.

## **1.2. Objective of Research**

This work presents a methodology of design and manufacturing the variable stiffness cellular structure. The mechanical property interested in this research will be the elastic property of cells under out-of-plane compression load.

First objective is to extract property information from performance distribution map by utilizing the image analysis technique with MATLAB. Image will be quantized and the color will represent the local property.

Design and analysis of unit cells will be the second objective. The parameters of the unit cell will be defined first, and by change one parameter every time, test and record the mechanical performance at that level. The relationship of the mechanical performance and unit cell parameter should be provided after this step.

Known the relationship of parameters and mechanical performance, voxelization will be done first to decide the unit cell size. Different unit cells can have different methods of voxelization, each need to be studied according to their geometry properties. A map of voxels will be the output of this step.

The last step of design is to fit the unit cells into the vary-sized voxels. An evaluation should be given for validation.

## **1.3. Overview of Research**

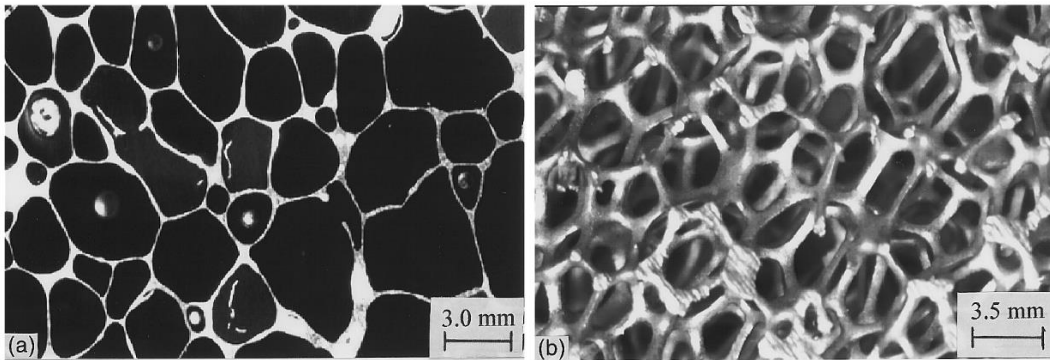
This thesis is presented in the following order: Chapter 2 includes all the background study and literature review of cellular structure and their fabrication methods. The proposed method will be detailed introduced in Chapter 3 & 4 for two types of cells including data extraction, unit cell

parametrization, voxelization and cell fitting. The proposed method will then be implemented to design an ergonomic mattress in Chapter 5, and evaluation is also given by compare the design with existing mattress. Conclusion with recommended future work is listed in Chapter 6.

## 2. LITERATURE REVIEW

### 2.1. Cellular Structure

Cellular structure has been defined as “an assembly of cells with solid edges or faced, packed together so that they fill space” by Gibson, and this type of material are common to see in nature, including sponge, wood and coral, etc. (L. J. Gibson & Ashby, 1999). These natural materials are found to be highly material and mechanically efficient. People start design their own cellular structures with the inspiration of these materials. Human made cellular structures are introduced in many application and area including high stiffness structures (Bauer, Hengsbach, Tesari, Schwaiger, & Kraft, 2014) , energy absorption (Ajdari et al., 2011), thermal insulation (Valdevit, Pantano, Stone, & Evans, 2006) and bio-printing (Ahsan et al., 2017) . Cellular structures are classified into 3 categories as shown in Figure 1: open cell, closed cell and combination of open and closed cells.



*Figure 1.* Examples of cellular material (A-M Harte, Fleck, & Ashby, 1999): (a) closed cell alporas foam and (b) open cell duocel foam.

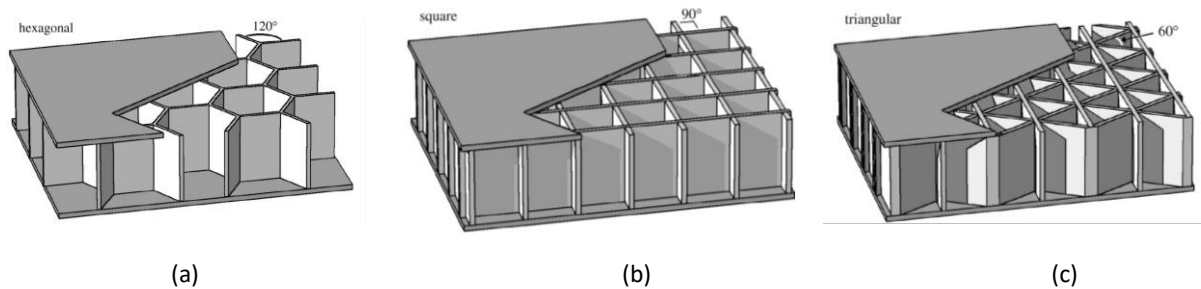
An important feature used to define a cellular structure is its relative density,  $\rho^*/\rho_s$ ; which is the ratio of the cellular structure density,  $\rho^*$ , and the density of the solid made with the same material,  $\rho_s$ . Closed cells usually has higher relative density compare to open cells. As the relative



density increases, the thickness of the cellular structure wall will be increased and pore size will be reduced.

### 2.1.1. Closed Cell

“If the faces are solid so that each cell is sealed off from its neighbors, it is said to be closed-celled” (L. J. Gibson & Ashby, 1999), no air flow along the in plain direction. The most known closed cell structure can be the honeycombs which has been widely used as the core of sandwich structures, floating structure, and packaging. Figure 2 shows some example of honeycomb structure.

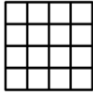

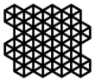
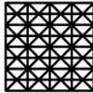
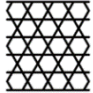
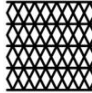
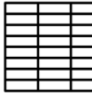









*Figure 2.* Examples of three types of honeycomb as core in sandwich structures (Wadley, 2006): (a) hexagonal honeycomb, (b) square honeycomb and (c) triangular honeycomb.

There are more cell types can be used as the core structure of sandwich honeycomb, Table 1 gives cross sections of different types of cell shape and their relative density equation (Wang & McDowell, 2004). Different cell shapes are preferred for different applications with their unique geometry properties. For example, hexagonal and rectangular cells are preferred for force convection and triangular cells perform better under in-plane compression.

Table 1

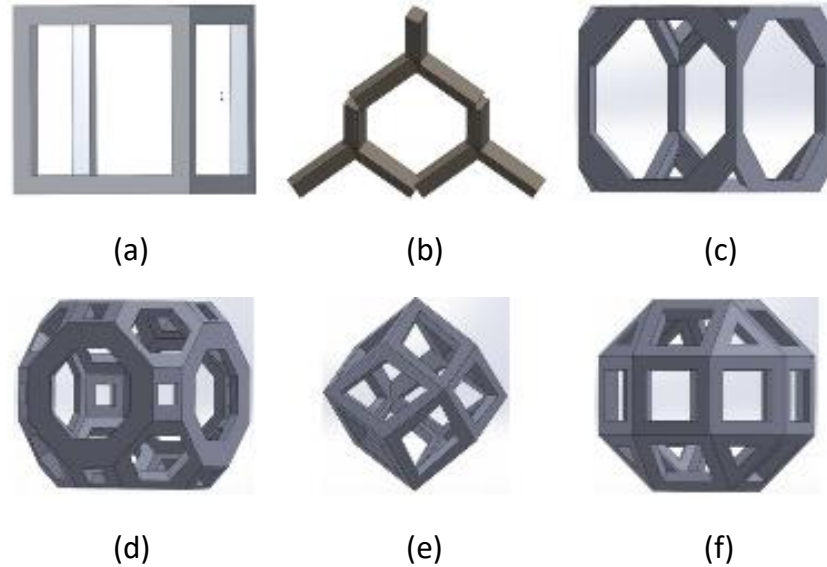
*Periodic Honeycomb Structures with Different Cell Types*

							
Unit Cell							
Cell Type	Square	Hexagonal	Equilateral triangles	Mix of squares and triangles	Kagome	Diamond	Rectangular
Relative Density	$\frac{2t}{\sqrt{3}l}$	$\frac{2t}{\sqrt{3}l}$	$\frac{2\sqrt{3}t}{l}$	$\frac{(2 + \sqrt{2})t}{l}$	$\frac{\sqrt{3}t}{l}$	$\frac{5t}{\sqrt{3}l}$	$\frac{(a + b)t}{ab}$

### 2.1.2. Open Cell

“If the solid of which the foam is made is contained in the cell edges only (so that the cells connect through open faces), the foam is said to be open-celled (L. J. Gibson & Ashby, 1999).” Open cells attracted more attentions recently with its lower relative density and various unit cell types with different mechanical properties. By changing the strut diameter and length, the relative density will be changed as well as the mechanical properties.

There are several approaches to make open cell structures. Metal lattice truss are usually made by investment casting which introduce rapid prototyping methods to create the patterns and casting with liquid metal. People also use weaving and braiding of wires to provides simple metal trusses. In addition, 3D printing also has been applied to make open cells including selective laser melting (SLM) (Ahmadi et al., 2015) and selective laser sintering (SLS) (Maskery et al., 2017).The fabrication methods will be introduced in detail in Chapter 2.2. Figure 3 gives some example of unit open cells.



*Figure 3.* Schematic drawings of six type unit open cells in cellular structure (Ahmadi et al., 2015): (a) cubic; (b) diamond; (c) truncated cube; (d) truncated cuboctahedron; (e) rhombic dodecahedron; (f) rhombicuboctahedron.

## **2.2. Fabrication Methods of Cellular Structure**

### **2.2.1. Closed Cell Fabrication**

Metal honeycomb sandwich structures are widely applied in industries. People has designed and applied many different process to manufacturing honeycombs which are repeating the unit cell in two dimensions to create the 3D structure. However, each process will have some limits either on the relative density or cell type which will be detailed introduced below in this chapter.

#### ***2.2.1.1. Hexagonal***

A most known method to fabricate hexagonal honeycomb is called expansion manufacturing process (Wadley, 2006). Thin metal sheets firstly been cut into panels, and bent into desired shape, aligned strips will be bonded together by laser welding to form a HOBE block. Then the block can be cut into desired length and stretched to form the hexagonal shape. But the

stretch process has high requirements on the bonding strength and stretch force. So this method is only suitable for low relative density structures.

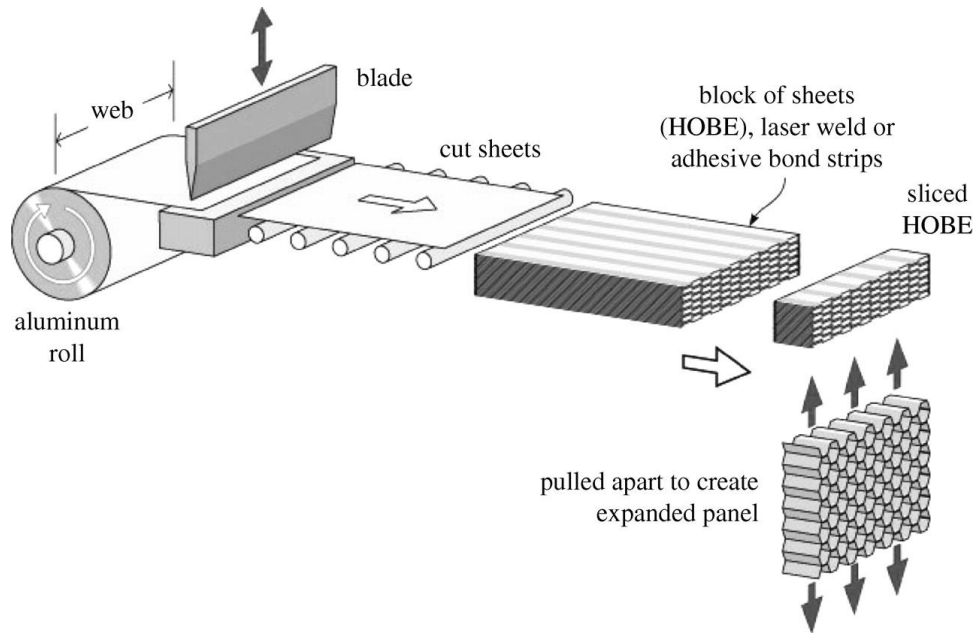


Figure 4. Illustration of expanded honeycomb manufacturing process (Wadley, 2006).

To manufacturing high relative density hexagonal structure, corrugation process is applied. The difference is that corrugation of metal sheet will be done first before cut and bonding. And residence welding is used for bonding layers together to form the hexagonal shape. No stretch needed in this process then. However, both of these two processes need to spend long time in bonding process. And bonding two layers together will change the equivalent thickness of the edges, which causes the loss of isotropic in hexagon shape.

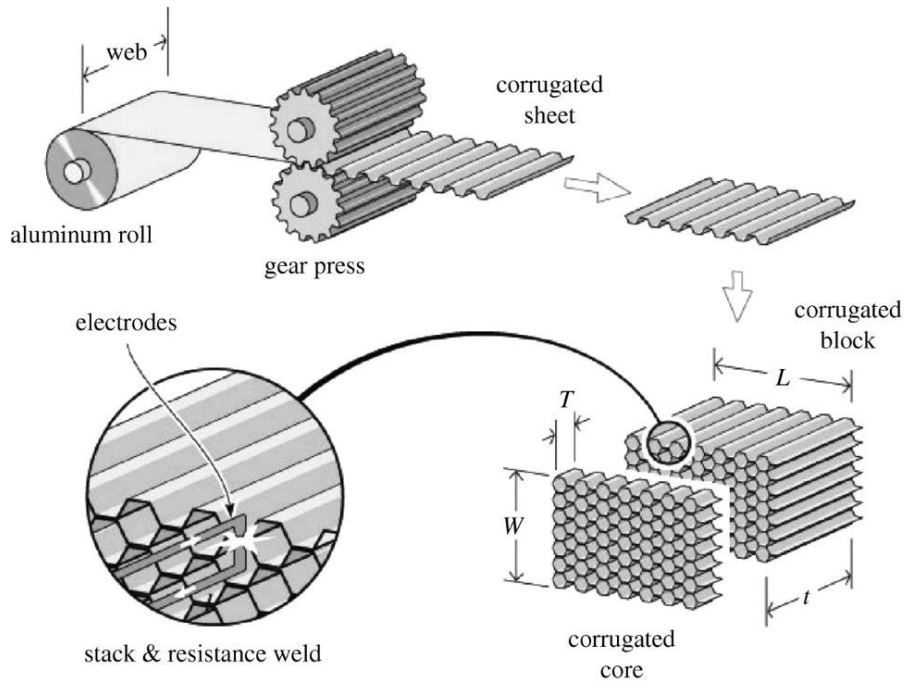


Figure 5. Illustration of corrugation manufacturing process (Wadley, 2006).

### 2.2.1.2. Prismatic Topologies

Similar to the corrugation process for hexagonal, the process can be applied to manufacture triangular, square or flat topped prismatic structures as well when the relative density is low. But slotted sheet method is preferred in manufacturing high-relative-density prismatic topology structures. Figure 6 is shown the process of fabrication of square and triangular honeycomb cores. The strips are bonded by brazing.

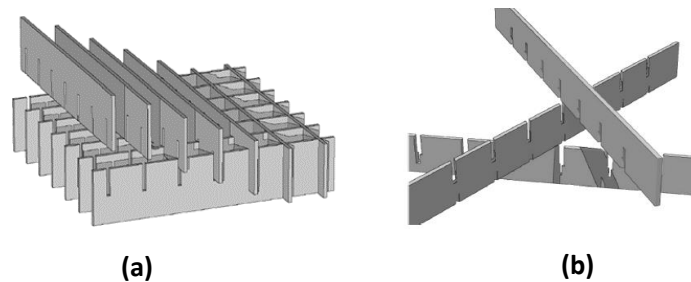


Figure 6. Illustration of strip slotting method (Wadley, 2006) for making (a) square honeycomb and (b) triangular honeycomb.

Even though this process has no bending process which can be used for less ductile materials. But only certain prismatic topologies (square, triangular) can be made with this method.

### 2.2.2. Open Cell Fabrication

Open cell fabrication methods are usually more complicated compare to closed cell. Below in Figure 7 shows a method of making pyramidal lattice structure. Metal sheets are perforated by laser or water jet cutting to create diamond shape holes, and then folded along nodes to create the 3D pyramidal shape. The same process can be applied to make tetrahedral structure when hexagonal pattern is perforated. But it's easy to figure out that the waste of material in this method is a lot and as the relative density decreases, the waste of material will significantly increases.

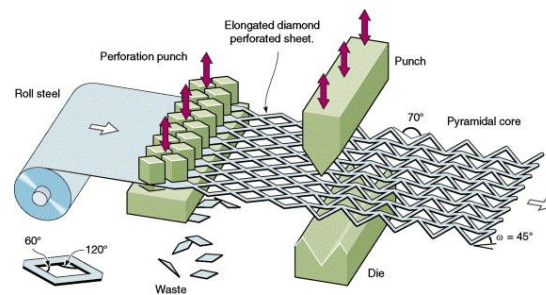


Figure 7. Illustration for the manufacturing method of pyramidal cores (Kooistra & Wadley, 2007).

Open cellular structures that have textiles topology can be made by wire lay-up process shown in Figure 8. Slotted tools are used to control the space between wire and their orientation. And then lay down the wires into the slots and reverse direction in next layer. Repeating the same process until desired thickness (number of layers). This method can only be used to fabricate square or diamond topology structures. And precise location of slotted tools needs to be achieved.

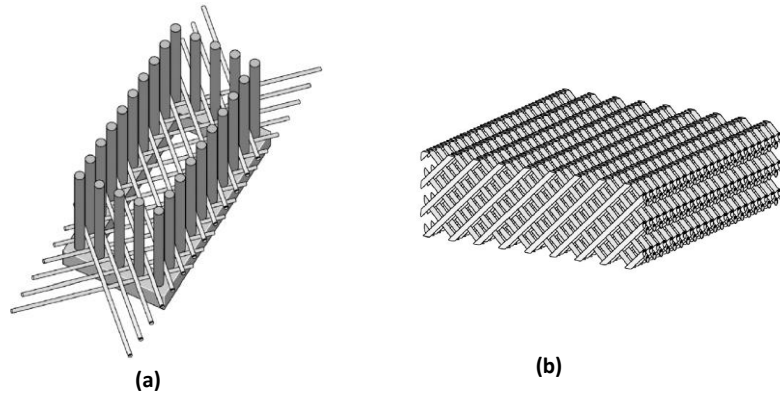


Figure 8. Wire lay-up process (Wadley, 2006) (a) layup wire, (b) core wires bonded and cut.

Additive manufacturing methods also been applied in the fabrication of cellular structures, Ahmadi used Selective laser melting (SLM) to create cellular structure with biomaterials (Ahmadi et al., 2015). Bauer applied laser lithography to fabricate high strength cellular structure with ceramic powder (Bauer et al., 2014). Fused deposition modeling (FDM) also been used for cellular structure fabrication. However, the layering effect caused a relatively higher possibility of failure as shown in Figure 9. And most of the 3D printing technologies has higher limits on the type of material.

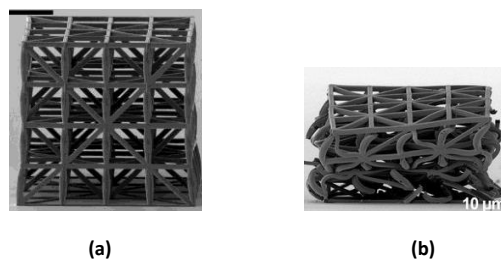


Figure 9. Cellular structure with AM (a) CAD model of cellular structure, (b) failed sample (Bauer et al., 2014).

### 3. TOPOLOGY DESIGN FOR CLOSED CELL

In this thesis, a methodology is proposed to design the variable stiffness cellular structure as shown in Figure 10, performance distribution map will be used as input for image analysis to extract the digitized performance information. And after define the parameter of unit cell, a study will be given on the cell performance based on the cell parameter. The information gathered from these two step will be used to voxelize the design domain. Unit cells will be fitted to the vary-sized voxel respectively.

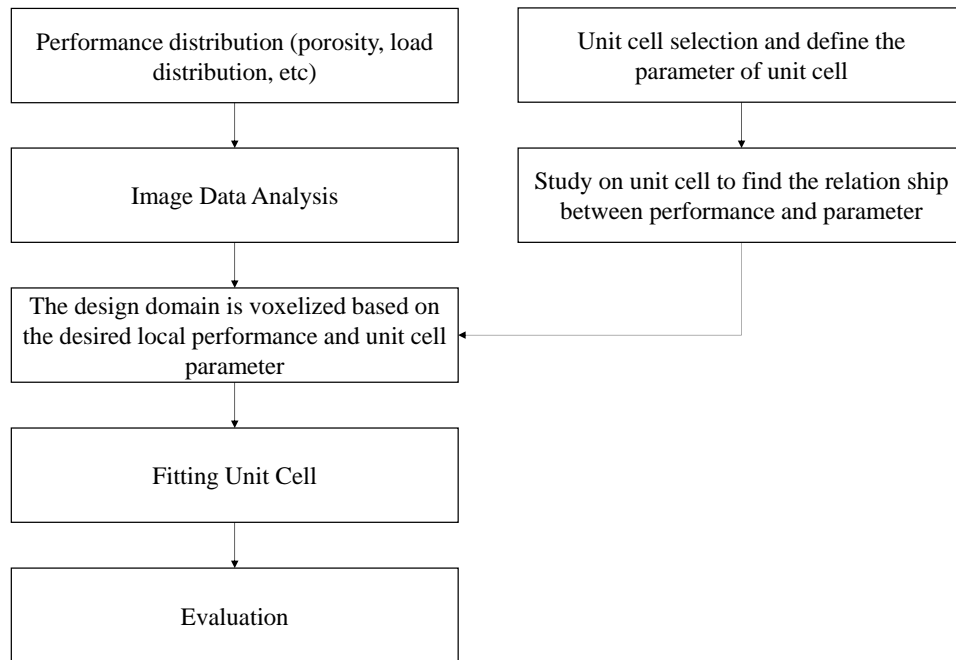


Figure 10. Flow diagram of proposed methodology.

#### 3.1. Image Performance Data Extraction

Performance distribution of objects are stochastic which provides multi-functionality such as mechanical and biological and so on. Images that contains the property information obtained from the sensors or simulations can be analyzed to model the heterogeneity of the object. The image will be converted to colored image if it is grayscale and the color information represents the



property. Pixel color information will then be extracted and quantized to be used as the measure of property.

An image is used here to show the heterogeneity, and the property we interested to mimic is the porosity. The grayscale image is an array of pixels  $P_{x,y} = [P_{x,y}]$ , where  $P_{x,y}$  is the intensity value of the pixel at location  $(x, y)$ . The pixel values varies spatially and can be mapped as a function of  $x$  and  $y$ , so the image will be represented as a single value function  $I : [1, \dots, m] \times [1, \dots, n] \rightarrow \mathfrak{R}$ , where  $m$  and  $n$  are the pixel numbers along  $X$  and  $Y$  directions, respectively.

The pixel intensity values of image  $I$  were then discretized through image quantization. In order to do that, the grayscale image will be converted into colored image first with a user defined quantization levels ( $l$ ), the image  $I$  was transformed into  $I' : [1, \dots, M] \times [1, \dots, N] \rightarrow [1, \dots, l]$  taking only a discrete finite set of pixel values, Figure 11 showed this process with ( $l = 8$ ). In fact, higher value of  $l$  means more quantization levels can increase the accuracy of the property information while take longer process time. This process resulted in a set of discrete iso-intensity value regions in the image. In fact, this pixel value region in an image can be assumed to possess approximately same microstructural heterogeneity.

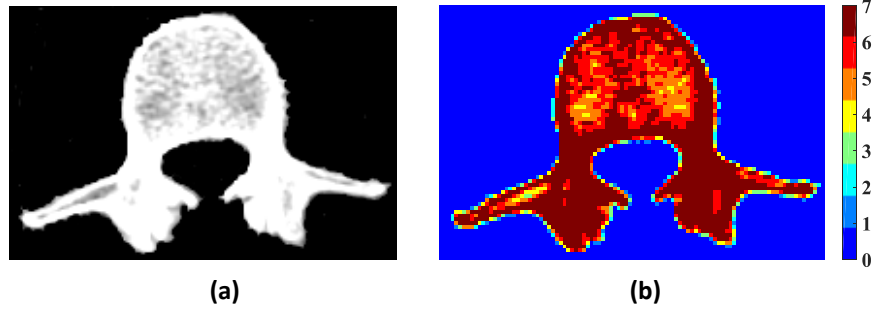


Figure 11. (a) Image with heterogeneous porosity, (b) corresponding quantized images with  $l = 8$ .

### 3.2. Relationship between Unit Honeycomb Cell Performance and Parameter

After reading the property information from the input image, we have to decide which type of cell will be used to fill the space and satisfy the property requirements. In this part, regular hexagonal honeycomb structure will be studied and analyzed to figure out the relationship between the parameters and their elastic properties.

#### 3.2.1. Gibson-Ashby Model of Cellular Structure Deformation

Gibson and Ashby (L. J. Gibson & Ashby, 1999) provided the equations of the relationship between the mechanical properties and their relative density after an extensive study of different structures. Cellular structures are known to have three stages deformation under the compression load. In this study, only the elastic region will be studied and the equation from Gibson is given below.

$$\frac{E^*}{E_s} = C_1 \left( \frac{\rho^*}{\rho_s} \right)^n \quad (1)$$

Where  $E^*$  is the Young's modulus of the cellular structure,  $E_s$  refers the Young's modulus of the material. This relationship equation is then reproduced in Equation 2 to find the direct relationship between the relative densities of the Young's modulus for a certain material.

$$E^* = E_s * C_1 \left( \frac{\rho^*}{\rho_s} \right)^n = C_2 \left( \frac{\rho^*}{\rho_s} \right)^n \quad (2)$$

And from Gibson and Ashby, the exponents  $n = 1$  for closed cell, and  $n = 2$  for open cell.

$C_2$  includes all the geometric constants of proportionality.

### 3.2.2. Structure Characterization and Selection of Parameters for Regular Hexagonal

#### Honeycomb

As described in Chapter 2.1.1, Honeycomb structure is the most widely spread natural and man-made closed cellular structure. It has been selected as 3D printing infill pattern and core of sandwich structures in the past decades due to the high material efficient. Many researchers have studied and proved that honeycomb structures obtain high strength under both in-plane and out-of-plane loads (Wang & McDowell, 2004). Honeycomb cell shapes including square cell, equilateral triangles, regular hexagonal and diamond, etc. This research will only focus on regular hexagonal honeycomb which is a regular array of hexagonal prismatic nest together to fill a space. And its performance under out-of-plane (along longitudinal cell axes) load will be tested and analyzed. It is easy to prove that regular hexagonal honeycomb has lower relative density by analyze the geometry of regular hexagon and other shape including square, rectangle and triangle. With the same perimeter, regular hexagon will give larger area which indicates with same amount of material, hexagonal honeycomb structure can fill larger space than square cell or rectangular cell honeycombs.

Two parameters will be needed to define a regular hexagon, the length,  $l$  (mm) and wall thickness,  $t$  (mm), and these two parameters will be used to determine the relative density of the unit cell.

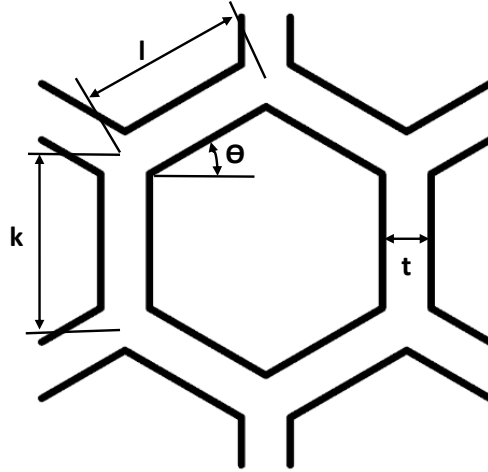


Figure 12. Hexagon parameters.

We now evaluate the relative density,  $\frac{\rho^*}{\rho_s}$  which is a function of the edge lengths,  $l$  and  $k$ , arbitrary cell wall angle  $\theta$  and thickness  $t$ , simple geometry gives the following relationship when neglect the quadratic term at low relative density (Wang & McDowell, 2004):

$$\frac{\rho^*}{\rho_s} = \frac{t/l(k/l + 2)}{2 \cos \theta (k/l + \sin \theta)} \quad (3)$$

Which reduces to:

$$\frac{\rho^*}{\rho_s} = \frac{2}{\sqrt{3}} \frac{t}{l} \quad (4)$$

When the cells are regular ( $h = l; \theta = 30^\circ$ ).

And the surface area  $A$  of a unit cell is given below.

$$A = \frac{3\sqrt{3}}{2} l^2 \quad (5)$$

### 3.2.3. Study on Unit Cell Parameter

Honeycombs are stronger and stiffer under out-of-plane load where only axial stress applied to the walls. Changing the thickness of the wall will cause the change of relative density

and mechanical properties. A compression test has been designed to figure out the relationship between Young's modulus and its relative density. The compression load is applied along Z direction as shown in Figure 13.

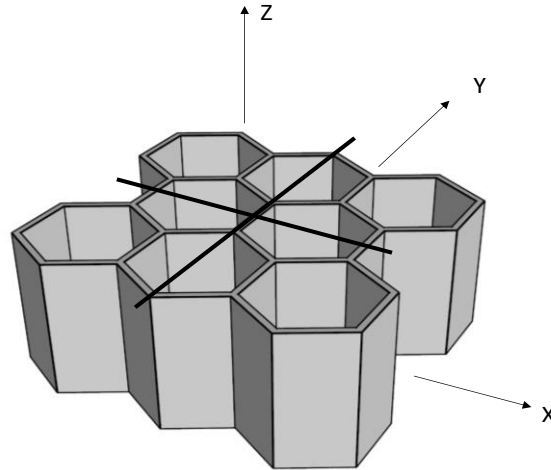


Figure 13. Compression load applied on hexagonal honeycombs along Z direction.

Test specimens were designed with eight hexagonal prismatic that has edge length of 20 mm, height of 45 mm and variation thickness as shown in the Table 2. The relative density were then calculated from the Equation 4 and listed below as well.

Table 2

*Design of Experiment of Regular Hexagonal Honeycombs*

Experiment	Edge Length(l) (mm)	Thickness(t) (mm)	Relative Density	Surface Area (mm <sup>2</sup> )
1	20	2	11.55%	8.7573E+3
2	20	3	17.32%	8.9816E+03
3	20	4	23.09%	9.2077E+03
4	20	5	28.87%	9.4355E+03

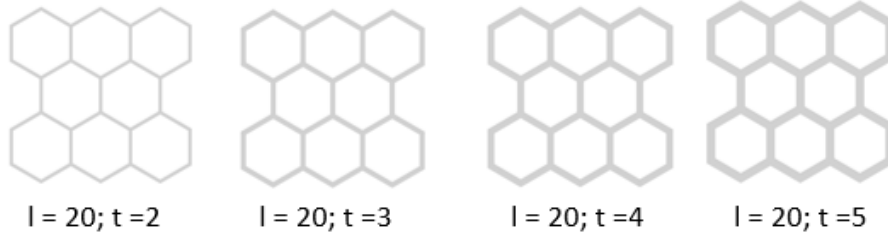


Figure 14. CAD file of the test samples with change on thickness (unit: mm).

### 3.2.3.1. Specimen Fabrication

Specimens were made by casting with Smooth-on Mold Star 15 Slow silicone which has a Young's Modulus  $E_s = 0.3792 \text{ MPa}$ , the molds were 3D printed with Makerbot Z18 printer. The design of the mold is shown in Figure 15 (a), inner hexagons were printed separately from the base and the boundary for easy demold. Bolts and nuts were used to locate the hexagons in right positions. The CAD models were then send to Makerbot Z18 printer to print. Vaseline is applied on the inner surface of the boundary and outer surface of hexagons to smooth the demold process. Silicones were poured into the mold with syringe and no degassing needed for this low viscosity rubber. The silicone needs 4 hours to cure at room temperature before demolding. To better keep shape of the samples, all specimens are left overnight for curing.

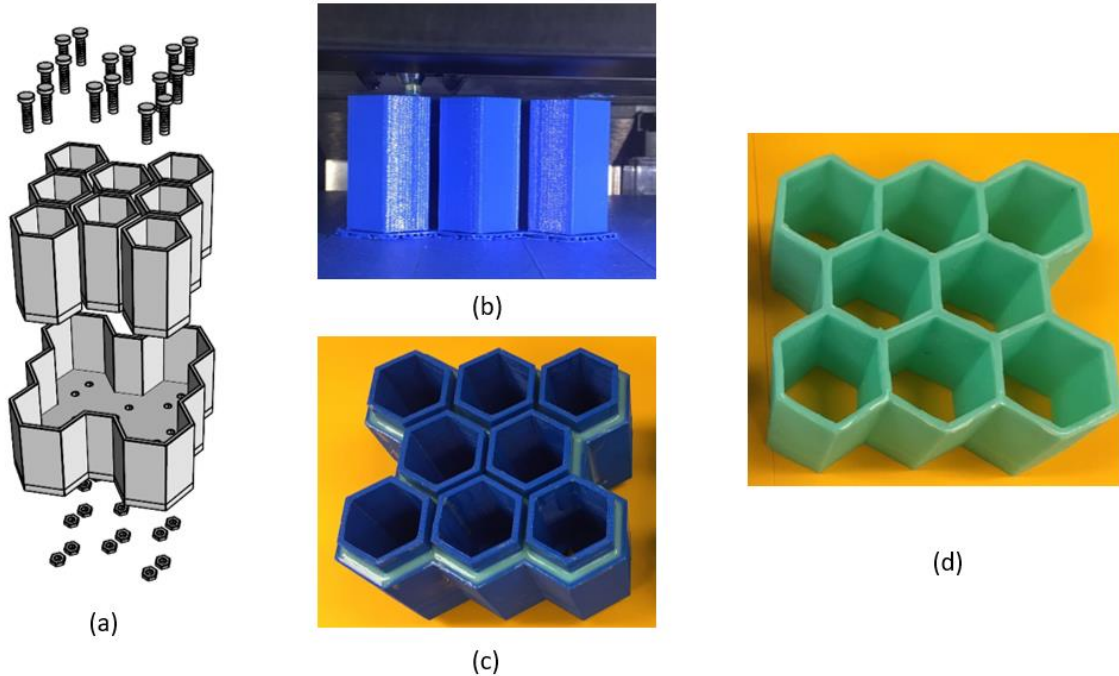


Figure 15. Specimen casting process: (a) the designed CAD model of mold, (b) mold printing with Makerbot z18, (c) pouring silicone with syringe into the mold, (d) demold the cast after curing for 4 hours.

### 3.2.3.2. Mechanical Test

Mechanical testing of the specimens was done with Instron 5567 universal test machine. The compression load is applied at the rate of 50mm/min along z direction until compressed 50% of original height (22.5mm). The deformations of a 5mm thickness specimen during the test are shown below in Figure 16.

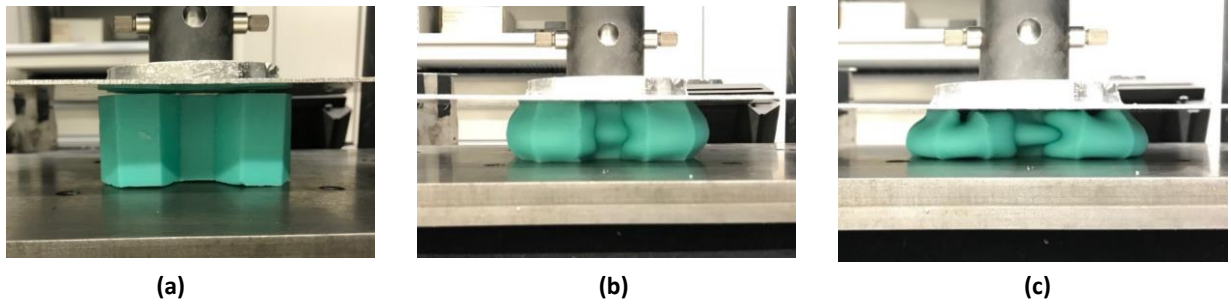


Figure 16. Compression test applied on silicone hexagonal structure (a) no load applied; (b) applying load to the structure; (c) 50% deformation happened to the structure.

The same tests applied to all the specimens successively with same machine setup to minimize the test-induced variation. And the results are shown below in Figure 17. The performances have larger variation when the relative density is lower but getting more stable when thickness increased.

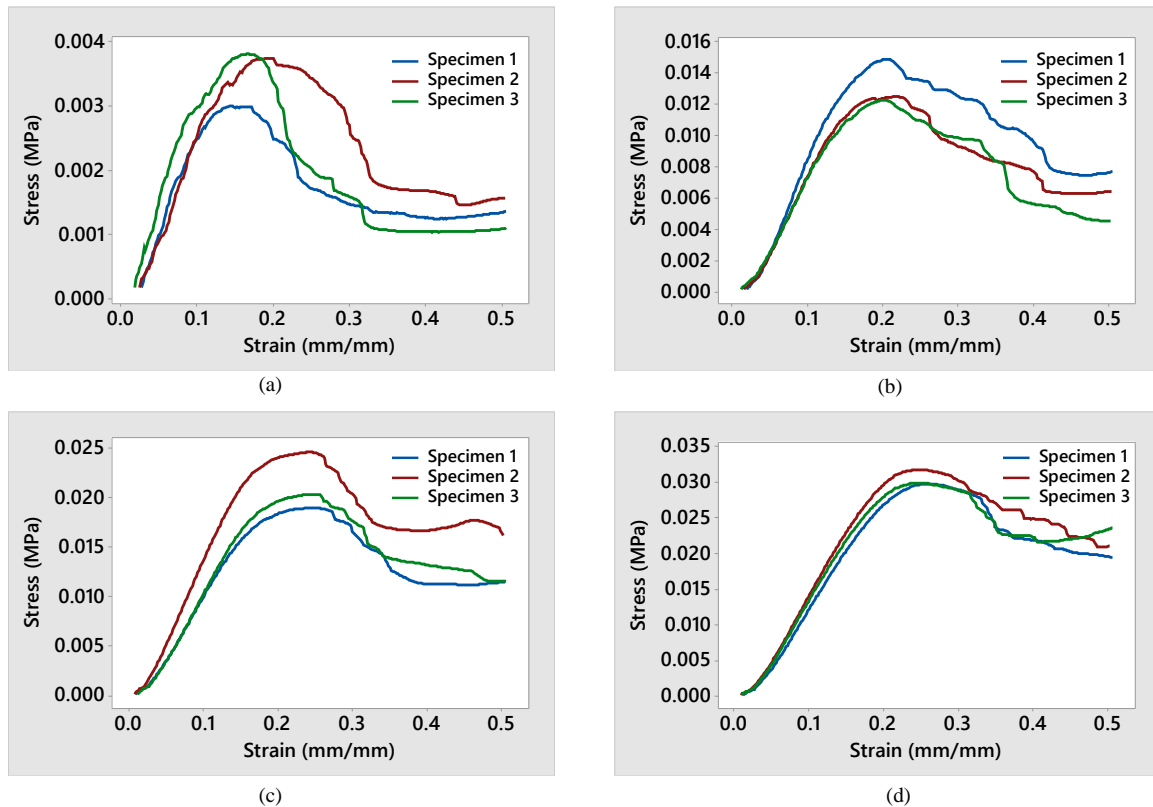


Figure 17. Compression test result of all specimens with different thickness, (a)  $t = 2$ , (b)  $t = 3$ , (c)  $t = 4$  and (d)  $t = 5$  (unit: mm).



This can be caused by different failure mode behaved during the compression test. We observed that all the specimens are failed because of buckling, but when the thickness is relatively low ( $t = 2mm$ ), it buckled inward. And when thickness increased to 3mm, some of the walls start buckled outward. As the wall thickness keep increasing, only outward buckling is shown under the test. This observation tells that the failure mode has some relationship with the wall thickness, and the change of buckling direction happened when the wall thickness is around 2mm and 3mm.

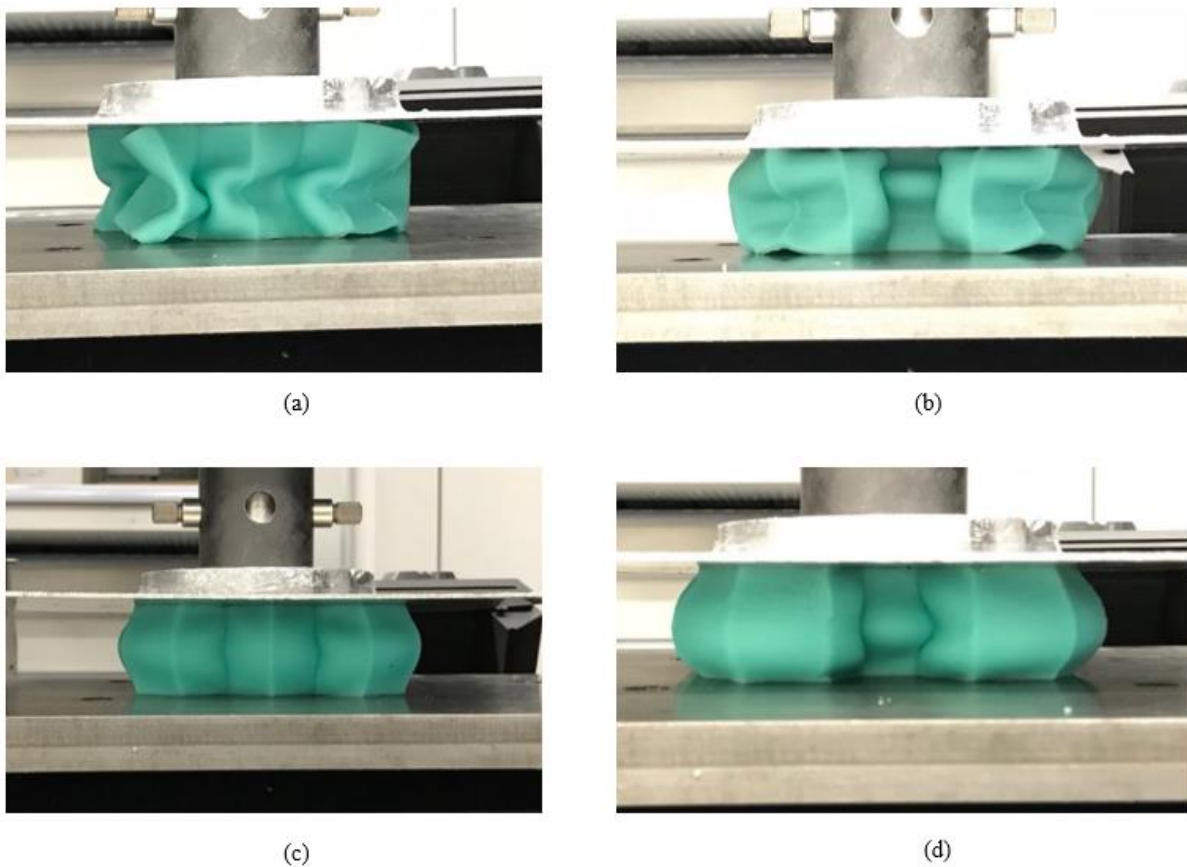


Figure 18. Failure mode for different thickness, (a) 2mm, (b) 3mm, (c) 4mm, (d) 5mm.

After the Stress Strain curves are fitted, Young's modulus of all the specimens will be found by using Equation 6 where  $\sigma(MPa)$  is the stress and  $\varepsilon(mm/mm)$  is the stain under the compression load,  $F$  is the load applied on the sample and  $A$  refers the apparent area of the sample which is the area closed by the boundary. Apparent area is a function of the cell edge length and

thickness as shown in Equation 5.  $\Delta h$  is the deformation happened with the corresponding  $F$ ,  $h$  is the height of the hexagonal prismatic.

$$E^* = \frac{\sigma}{\varepsilon} = \frac{F/A}{\Delta h/h} \quad (6)$$

The Young's modulus is actually the slope of the first stage deformation, the results are listed below in Table 3, mean value of three specimen are calculated for each sample and used as the modulus for that thickness were plotted in Figure 19.

Table 3

*Young's Modulus of All Silicone Hexagon Specimens*

Wall Thickness (mm)	Relative Density	Young's' Modulus (MPa)			
		Specimen 1	Specimen 2	Specimen 3	Mean
2	0.1155	0.025	0.025	0.0304	0.0268
3	0.1732	0.1025	0.0842	0.0801	0.08893
4	0.2309	0.1197	0.1225	0.1516	0.13127
5	0.2887	0.1527	0.1714	0.1644	0.16283

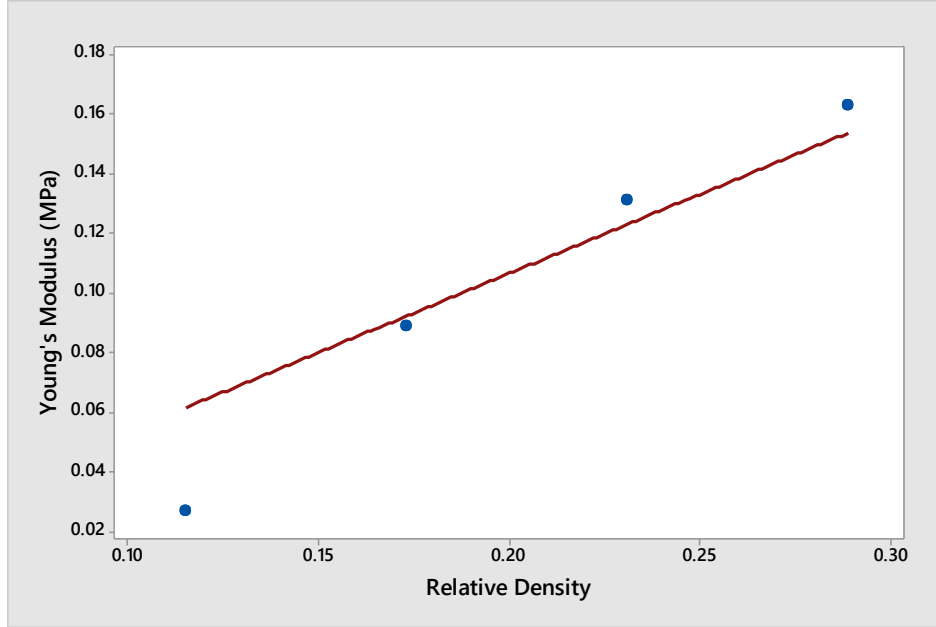


Figure 19. Plot of the Young's Modulus vs relative density for silicone hexagonal samples.

After plot the four points, a nonlinear pattern is observed, but as discussed, this can be caused by different failure modes when the thickness is low. For simplicity, a linear model was generated in this study with Minitab, A regression model  $E^* = 0.5323 \left( \frac{\rho^*}{\rho_s} \right)$  with  $R^2 = 97.39\%$  and  $P = 0.002$  is given. This model will be used to represent the relationship between the Young's Modulus and the relative density for this silicone hexagonal honeycomb.

### 3.3. Voxelization

After getting the property information from the image and known the relationship between the property performance and its relative density. The method of voxelization was introduced here to determine the cell size.

As introduced in 3.3.2, only the thickness of the hexagon structure ( $t$ ) is changed here to change the relative density and resulting the change of the mechanical properties. A hexagon

prismatic is made with two wall of hexagons as shown below. Two bounding box will be needed to define the thickness of the hexagon which is the offset distance between the two bounding box.

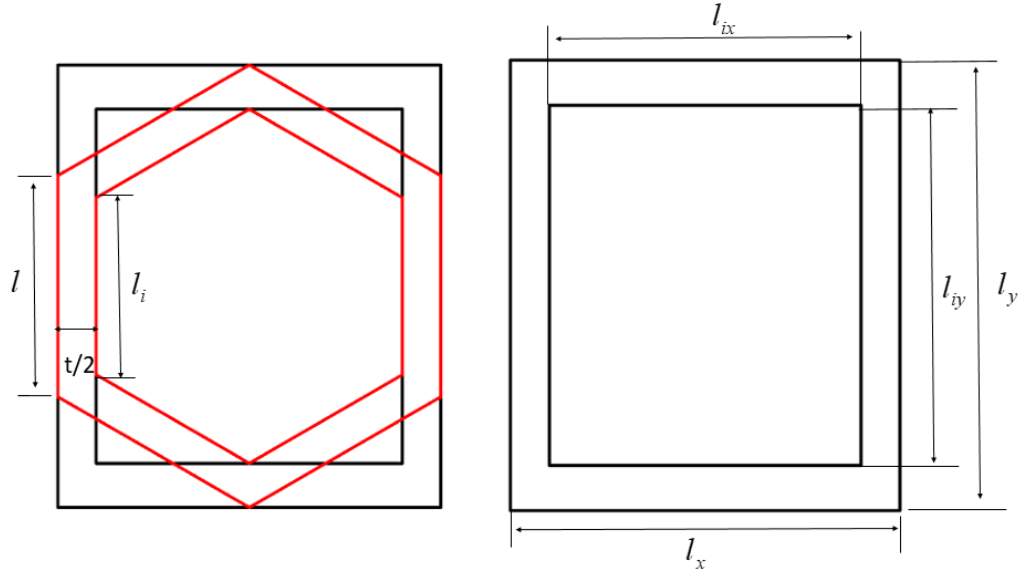


Figure 20. Voxel size parameters.

For a give cell length  $l$  , the bounding box parameter  $l_x$  and  $l_y$  can easily calculate from the following Equation 9. All the pixels values inside this bounding box will be found as  $I'_1 \rightarrow [P_x, \dots, P_{x+m_1}] \times [P_y, \dots, P_{y+n_1}]$  where  $m_1$  and  $n_1$  are the number of pixels along  $x$  and  $y$  direction, respectively. Then find the average pixel value  $\bar{P}_{x,y} = \frac{1}{m_1 n_1} \sum_x^{x+m_1} \sum_y^{y+n_1} P_{x,y}$  which will be used as the property indicator. And combine Equation 2, 4 and 5, we can find that  $t$  is a function of load and deformation happened at that location as represent in the following Equation. So with the information got from the image and this relationship, we can easily find the thickness for this voxel.

$$t = \frac{Fh}{3l\Delta h C_2} \quad (7)$$

After calculated the thickness, the inner hexagon size can be determined using Equation 8.

And the voxel parameter  $l_{ix}$  and  $l_{iy}$  will be calculated from Equation 10.

$$l_i = l - \frac{t}{\sqrt{3}} \quad (8)$$

$$l_x = \sqrt{3}l; l_y = 2l \quad (9)$$

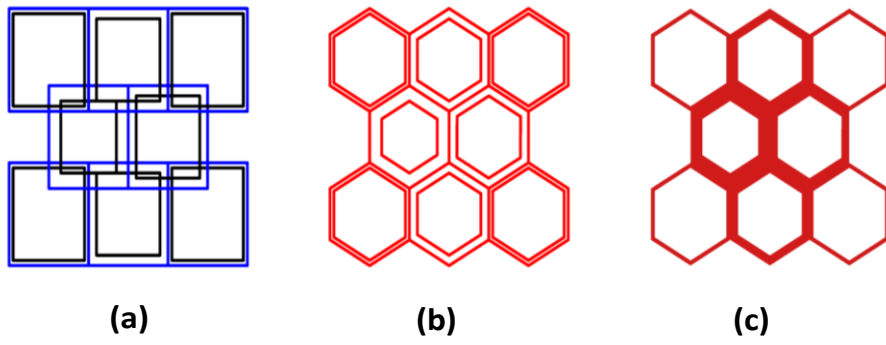
$$l_{ix} = \sqrt{3}l - t; l_{iy} = 2l - \frac{2t}{\sqrt{3}} \quad (10)$$

### 3.4. Fitting Unit Cell

This step is a reverse of the first part voxeliaztion. With given voxel size, we need to fit the unit cells into the voxel.

Figure 21 shows an example of fitting hexagons into the voxels. Figure 21(a) is the designed voxels where blue boxes are the outer box and blacks are the inner ones, hexagons will then be drawn using the Equation 11. Fill the space between two hexagons will create the walls of the hexagonal honeycomb.

$$l = \frac{l_x}{\sqrt{3}}; l = \frac{l_y}{2} \quad (11)$$



*Figure 21.* Hexagon unit cell fitting into voxel, (a) an example of voxelization result, (b) hexagon outlines are drawn with the equation, (c) the real honeycomb structure with variation thickness.

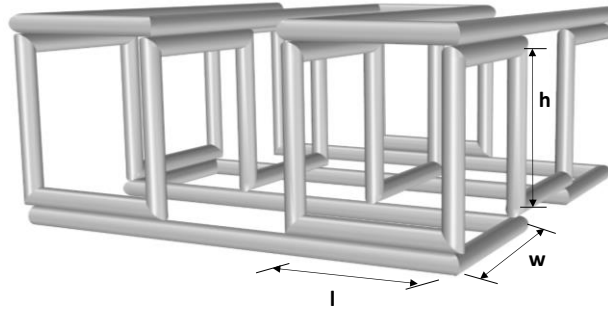
## 4. TOPOLOGY DESIGN FOR OPEN CELL

Similar to the Chapter 3, the same methodology will be applied to open cells, in this chapter, a new designed cuboid cellular structure was studied. And the proposed fabrication method of this metal cellular structure was introduced as well. Since the image data extraction will be same for this design, we only focused on the parametrization, voxelization and fitting cells for the cuboid cellular structure.

### 4.1. Relationship between Unit Cuboid Cell Performance and Parameter

#### 4.1.1. Structure Characterization and Selection of Parameters

Four parameters will be introduced here to determine the size of the unit cell as shown in Figure 22. The cell length ( $l$ ), cell width ( $w$ ), cell height ( $h$ ) and the metal wire diameter ( $D$ ).



*Figure 22.* Cuboid parameters.

There are several types of unit cells in this structure, to figure out the relationship between the parameters and relative density, every unit cell is studied in a  $5 \times 5 \times 1$  structure. There were totally 6 types of cells shown in these 25 cells and the pattern is listed below.

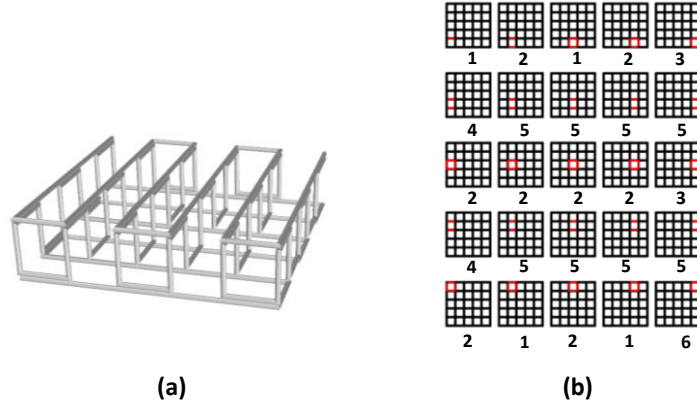








Figure 23. (a) CAD model of  $5 \times 5 \times 1$  structure, (b) study of each single unit cell and their cell type.

Table 4

*Analysis of Six Types of Unit Cells and Their Relative Density*

						
Cell Type	1	2	3	4	5	6
Times Appeared	4	8	2	2	8	1
Relative Density	$\frac{\pi D^2(2l + 2w + h)}{4lw(h + 3D)}$	$\frac{\pi D^2(l + 2w + h)}{4lw(h + 3D)}$	$\frac{\pi D^2(2l + 2.5w + h)}{4lw(h + 3D)}$	$\frac{\pi D^2(l + 2.5w + h)}{4lw(h + 3D)}$	$\frac{\pi D^2(l + 2w + h)}{4lw(h + 3D)}$	$\frac{\pi D^2(1.5l + 2w + 0.75h)}{4lw(h + 3D)}$

It is easy to find that only type 2 & 5 showed up in the center of the structure, other types are all on the edges, so as the structure getting bigger and more cells appeared in the structure, type 1,3,4 & 6 can be ignored. Since type 2 & 5 shared the same equation of relative density calculation. The equation will be used to determine the relative density of the unit cell.

$$\frac{\rho^*}{\rho_s} = \frac{\pi D^2(l + 2w + h)}{4lw(h + 3D)} \quad (12)$$



### 4.1.2. Study on Unit Cell Parameter

Only one parameter of cuboid cell will be selected to change during this study, from Equation 12, we found the width has higher weight compare to other two parameters. The target property is also the compressive elastic on the structures. The compression load is applied from the top, height direction.

The samples were designed to be  $5 \times 5 \times 1$  structures with edge length ( $l = 10mm$ ), cell height ( $h = 10mm$ ), wire diameter ( $D = 1.02mm$ ) and variable cell width as listed in Table 5. And 3 specimens are made for each sample.

Table 5

#### *Design of Experiment of Cuboid*

Experiment	Cell Length(l) (mm)	Cell Width(w) (mm)	Cell Height(h) (mm)	Metal Wire Diameter(D) (mm)	Relative Density
1	10	8	10	1.02	5.52%
2	10	10	10	1.02	4.90%
3	10	12	10	1.02	4.50%
4	10	14	10	1.02	1.20%

#### *4.1.2.1. Specimen Fabrication*

The highlight of this design is the continuity of the structure, the structure can be made with a single continuous wire. 18 Gauge copper wire was selected to make all the specimens. As shown in Figure 24, the structure is made of two layers of x-y plane zigzag and vertical walls of zigzag as core. The structure then been rotated to get a planar toolpath for machine to bend. A

desktop CNC machine is modified for the bending process. After the planar wire bended, manually bend the wire to 3D structures.

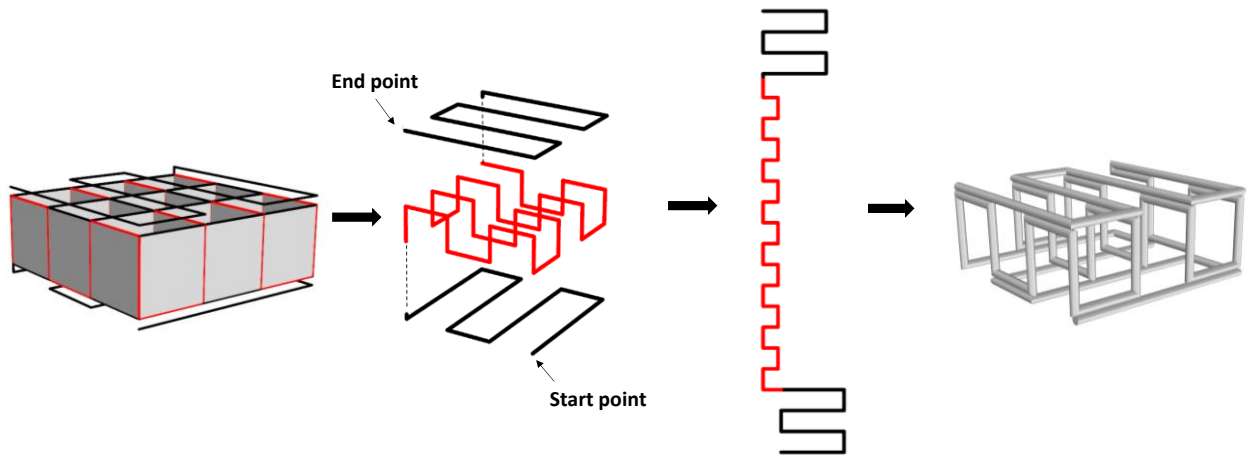


Figure 24. Wire bending process of making cuboid structures.

To enhance the strength of the structured, the specimens will be surfaced treated for better adhesive with a mixture of Nitric Acid, Ferric Chloride and distilled water as shown in Figure 25(b). Then the structure will be dipping into the epoxy and put in oven to cue. Compression tests are applied on the final structure as shown in Figure 25(c).

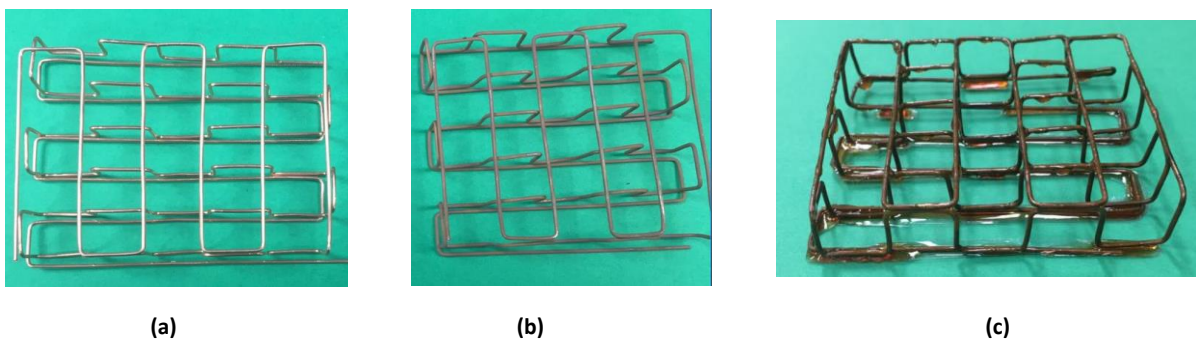
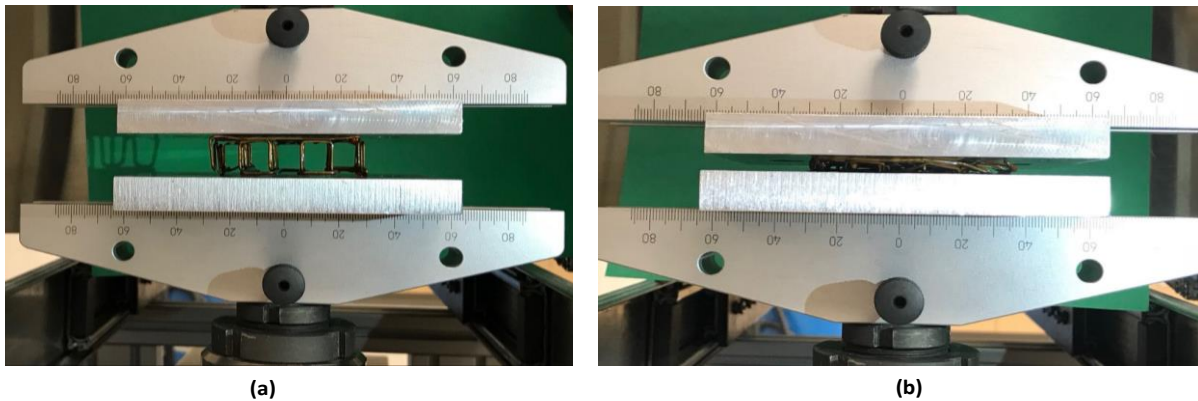


Figure 25. (a) Structure after bend, (b) structure after surface treatment, (c) structure after epoxy bonded.

#### 4.1.2.2. Mechanical Test

Mechanical test of the specimens was done by MTS Insight Electromechanical testing system. The compression load is applied at the rate of 15mm/min along z direction until 80% of deformation happened. The test deformation of a  $10 \times 8 \times 10$  specimen is given below.



*Figure 26.* Compression test applied on wire structure (a) structure before apply load, (b) 80% deformation happened.

Repeat the tests to all specimens without any change to the setup of the machine. The stress strain curves are drawn as shown below in Figure 27. The specimens have more sample variation compare to the hexagonal honeycomb. However, we also observed two types of failure mode in this structure. The buckling can be fan-spread as shown in Figure 28(a) that all the vertical truss are buckled toward outside, or it can be sway buckling as 28(b) that the truss are buckled toward one direction. Different failure modes can be the main reason of causing the specimens variation in the tests.

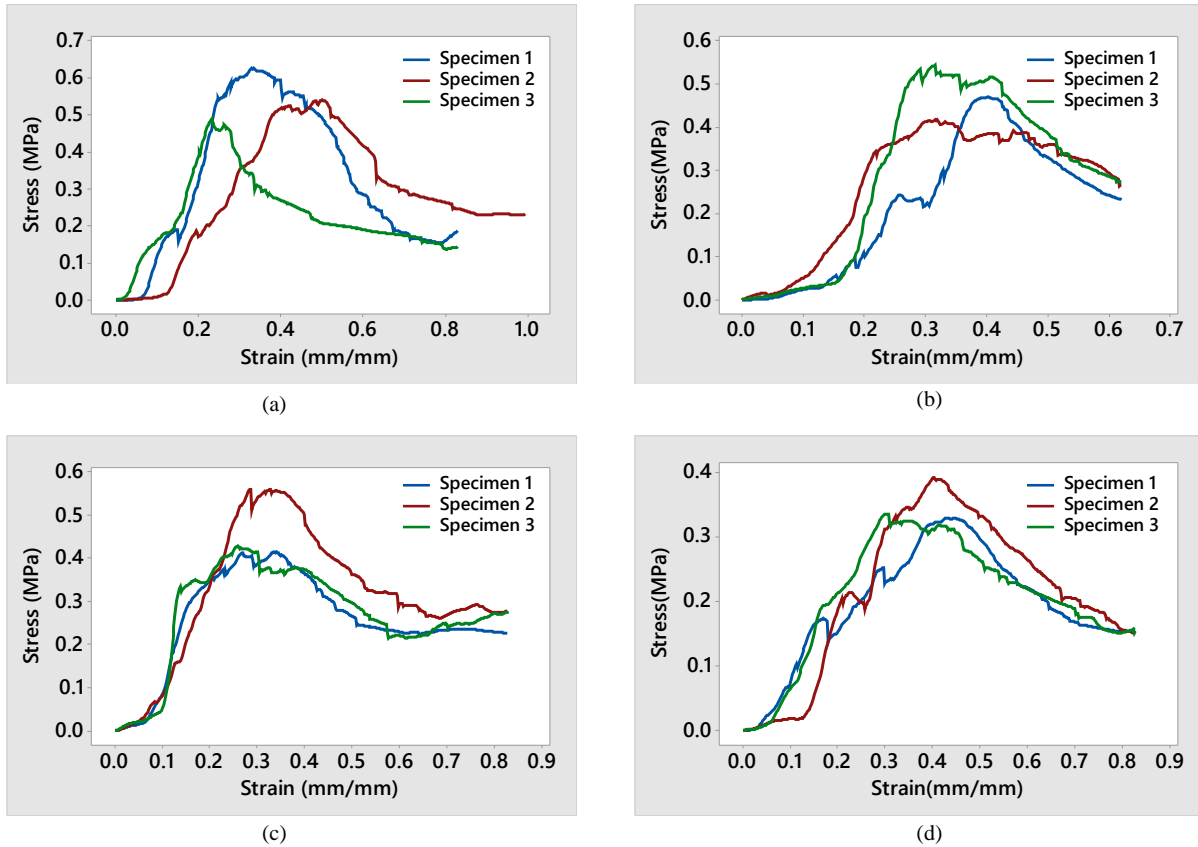


Figure 27. Compression test results of all specimens with  $l = h = 10$  , where (a)  $w = 8$  ; (b)  $w = 10$  ; (c)  $w = 12$  and (d)  $w = 14$  (unit: mm).

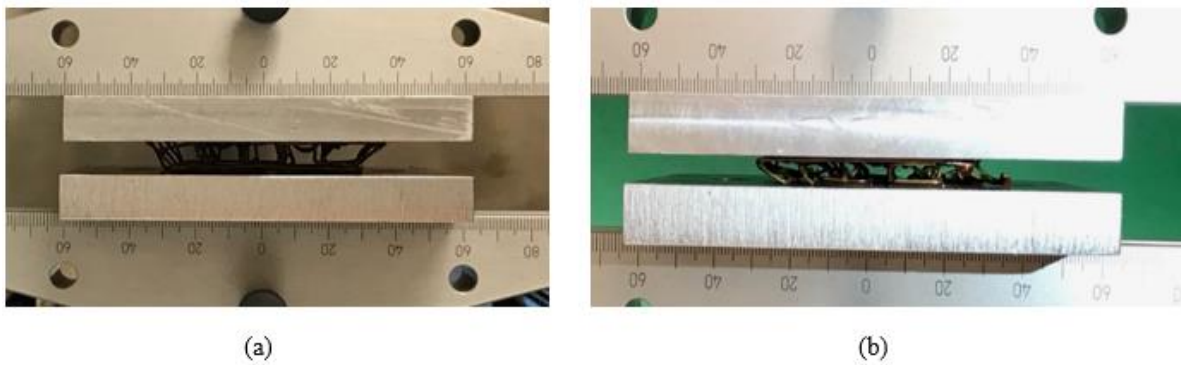


Figure 28. Failure modes of Cuboid Structure, (a) fan-spread buckling, (b) sway buckling.

Same as the hexagon structure, the Young's modulus of the specimens are calculated from Equation 6, and listed in Table 6. The mean value of 3 specimens for each sample is used to plot the Young's Modulus vs relative density figure and find the coefficient for the power law.

Table 6

*Young's Modulus of Wire Structures*

Cell Width(w) (mm)	Relative Density	Young's Modulus (MPa)			
		Specimen 1	Specimen 2	Specimen 3	Mean
8	0.0552	1.7377	1.4368	1.8541	1.6762
10	0.049	1.3758	1.4213	1.7307	1.5093
12	0.045	1.5628	1.4597	1.1934	1.4053
14	0.042	0.8031	0.9025	1.0397	0.9151

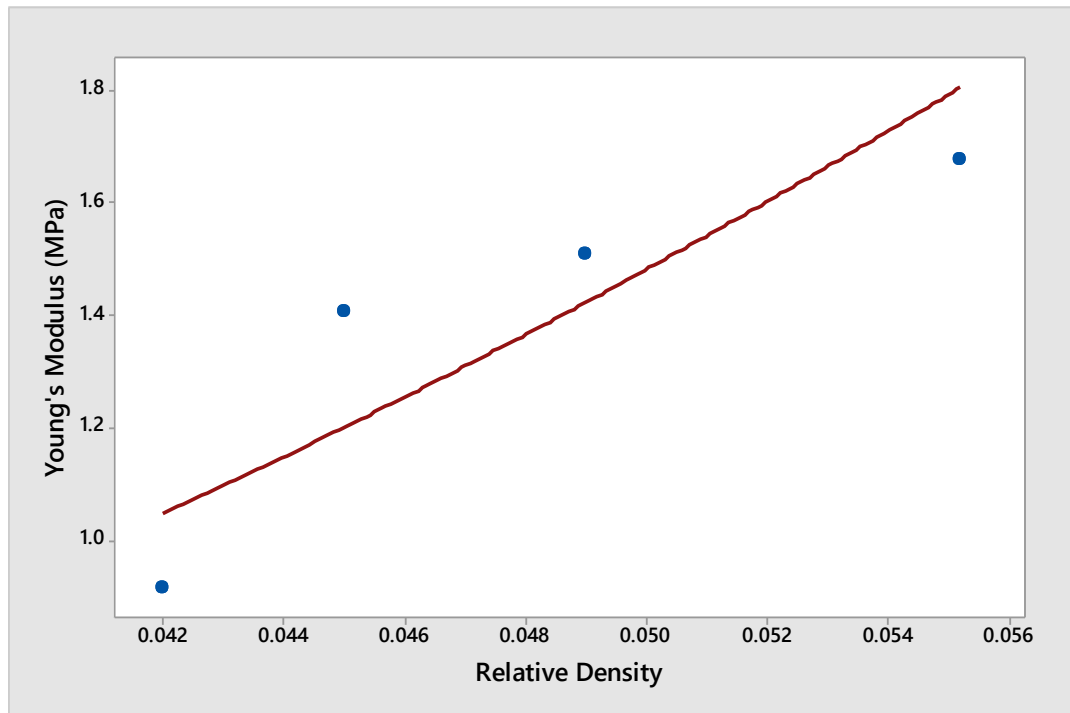


Figure 29. Young's Modulus vs relative density plot for wire structures.

From Gibson and Ashby, the exponents for open cells should be equal to 2. After plot the four points in the figure, we found this quadratic function did not fit perfectly with the data points.

We realized that this can be caused by missing of anneal process. The bending process actually

introduced strain hardening in bends, and the smaller the truss is, the higher effect will be. The mechanical properties will no longer stay consistent in the structure after bending. And since the size of structure are varied, the amount of Epoxy are also not equal on all specimens which can be another reason of causing the non-perfect fitting. But here again for simplicity, a fitted curve was

generated and analyzed in Minitab, The regression model  $E^* = 592.6 \left( \frac{\rho^*}{\rho_s} \right)^2$  with  $R^2 = 98.59\%$  and

$P = 0$  is given. This model will represent the relationship between the Young's Modulus and the relative density for cuboid structure.

#### 4.2. Voxelization

The only parameter used to determine the relative density as well as the mechanical property is the cell width for this type of cell. Since no height change introduced here, so the voxelization can be treat as 2D where the voxel parameter  $l_x$  and  $l_y$  are equal to the cell length  $l$  and cell width  $w$  respectively. The apparent area equation is give as well.

$$A = lw \tag{13}$$

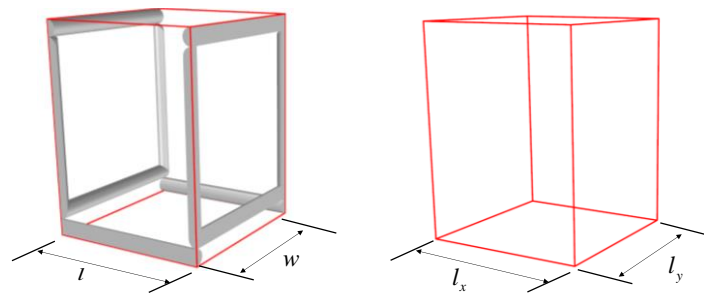


Figure 30. Cuboid voxel parameters.

Different from the voxelization of hexagon, the average pixel values  $\bar{P}_x = \frac{1}{N_y} \sum_y P'_{x,y}$  and

$\bar{P}_y = \frac{1}{N_x} \sum_x P'_{x,y}$  of the quantized image  $I'$  were firstly determined along both longitudinal (  $X$  )

and transverse (  $Y$  ) directions, respectively. Since the input is discrete function, adaptively

segmented but connected parametric polynomial B-spline curves  $\{C(u)\}$  are fitted to correlate the

average pixel values with spatial locations. The B-spline curve is a generalization of the Bézier

curve, i.e., Bézier curve is a B-spline with no interior knots(Piegl & Tiller, 1995).

$$\mathbf{C}(u) = \sum_{i=0}^n B_{i,n}(u) \mathbf{P}_i, \quad u \in [0, 1] \quad (14)$$

$$\text{where, } B_{i,n}(u) = \frac{n!}{i!(n-i)!} u^i (1-u)^{n-i}$$

Here,  $\{\mathbf{P}_i\}_{i=0,\dots,n}$  are the control points of the Bézier curve  $\mathbf{C}(u)$ . An example is given in

Figure 31 In this study, the control points of the Bézier curve are defined by the ordered pairs of

pixel location and pixel value,  $\{\mathbf{P}_i = (x, \bar{P}_x)_i\}$ .

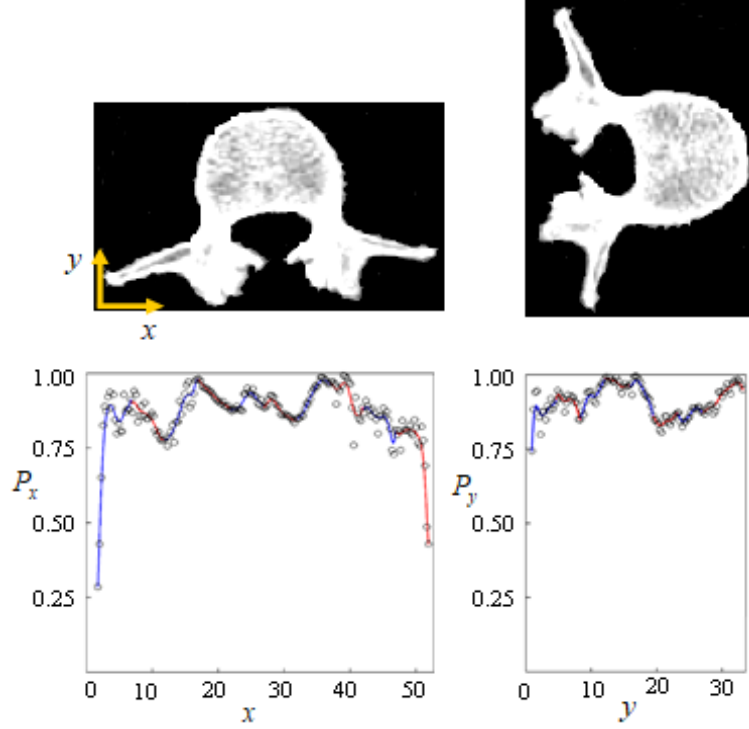


Figure 31. Parametric functions generated for the example image.

After fitting the Bézier curve, the voxel parameter  $l_x$  and  $l_y$  will be then determined. Since the cell length is not change, that means  $l_x$  will be a constant and only  $l_y$  needs to be determine. But both can be obtained with same procedure describe below. Combine Equation 2, 4 and 12, the cell width  $w$  is a function of the compression load and corresponding deformation.

$$\frac{(\pi D^2(l + 2w + h))^2}{14l^2w(h + 3D)} = \frac{Fh}{\Delta hIC_2} \quad (15)$$

$$l_x = l; l_y = w \quad (16)$$

In order to determine the voxel size, we firstly find the predicted property value  $\hat{P}_{y=0}$  when  $y = 0$  from the Bézier curves  $\{\mathbf{C}(u)^y\}$ . The  $\hat{P}_{y=0}$  will be fed into Equation 15 to find  $l_{y=0}$ . Then the  $x$  value will be updated to  $y = l_y$ ,  $\hat{P}_{y=l_y}$  will then been fed to find new  $l_{y=l_y}$ . Repeat the same procedure until the full image is mapped. Do the same process for  $x$  direction is needed. The



outcome of the above process will give a series of  $l_y$  and  $l_x$  which is the parameter of the voxel and an example of the voxelization for human vertebra is given below.

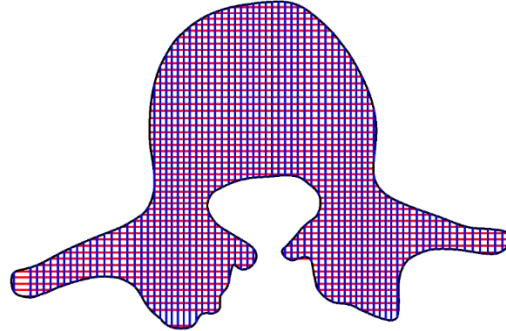


Figure 32. Example of voxelization.

### 4.3. Fitting Unit Cell

Figure 33 shows an example of a  $3 \times 3 \times 1$  cuboid cellular structure with variation size. Figure 33(a) is the designed voxelization from top view. Extrude the grid to create 3D voxels and fit the toolpath to generate the structure. The relationship between the voxel parameter and cell parameter is given in the Equation 17 below as well.

$$l = l_x; w = l_y \quad (17)$$

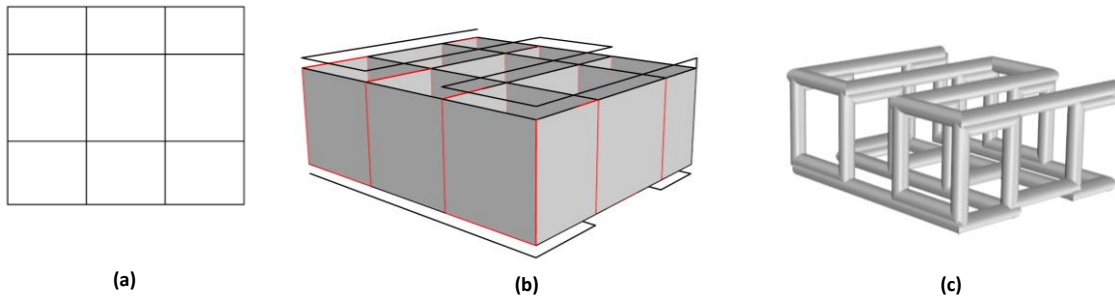


Figure 33. Cuboid unit cell fitted into voxels, (a) top view of an example of voxelization, (b) cells fitted into the 3d voxels, (c) CAD model of the variable sized cuboid cellular structure.

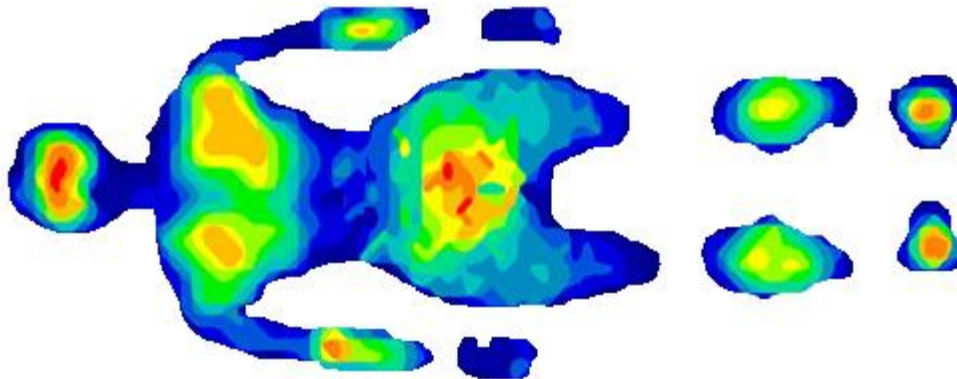
## 5. IMPLEMENTATION

### 5.1. Method Validation: Customized Mattress

People studied the sleep quality on different bedding system and figure out the design of the mattress and supporting system makes lot of difference in improve the sleep quality. A good sleep system should allow the muscles and intervertebral discs to recover from daily load (Nachemson & Elfstrom, 1970). This can be achieved when the shape of the spine is in its natural physiological shape. So the assessment of the sleep system support qualities is the spinal alignment. Two factors need to be considered for spinal alignment: spinal curve and weight distribution, since both of them are highly individual, a better sleeping system should on designed on a personalized basis (Haex, 2004).

In this chapter, the proposed method will be applied to design a customized mattress which use the information of the body shape of the customer and the load distribution map when sleeping on mattress.

A full body pressure distribution map gained by Tekscan's Body Measurement System("Pressure Imaging for Mattress Design," 2013) provides the data across the entire body in real-time 2D pressure displays. A pressure distribution map of human body on support surface (mattress) is given in Figure 34.



*Figure 34.* Load distribution map on mattress ("Pressure Imaging for Mattress Design," 2013).

The image was then discretized through image quantization, each color represents a level of load, an array of pixel color value  $P_{x,y}$  with size  $m \times n$  will be extract form the image as shown below in Figure 35.

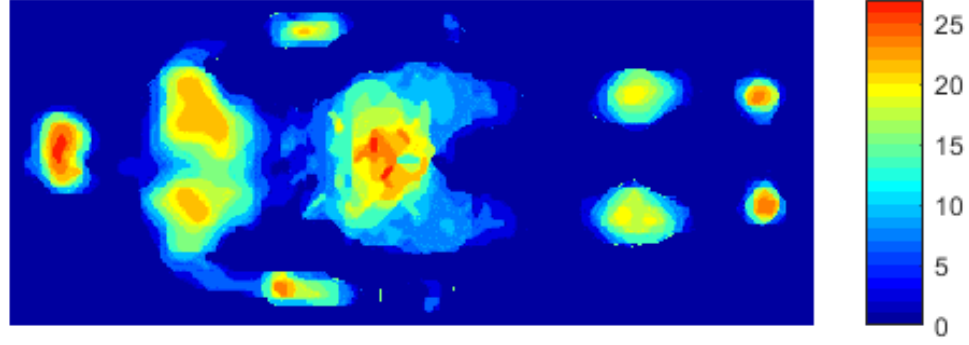


Figure 35. Quantized image, respectively at  $l = 32$ .

The total pixel value will then be calculated to figure out which color represents how much load. Assuming the tester of the image resource has weight of 180lb which will create 800N load when lying down on mattress. Then the step size of the quantization level  $s$  will be calculated from the Equation 18. So, the array of weight distribution along the mattress  $F_{x,y}$  will be figured out from Equation 19.

$$s = \frac{800}{\sum_{x=1}^m \sum_{y=1}^n P_{x,y}} \quad (18)$$

$$F_{x,y} = sP_{x,y} \quad (19)$$

As shown in Equation 8 that the voxel size is a function of the load and deformation, after gain the load distribution information, we need to find the corresponding deformation to determine the voxel size. Figure 36 shows some common postures human behaved and the perfect alignment to the normal ideal posture will be the target of this design.

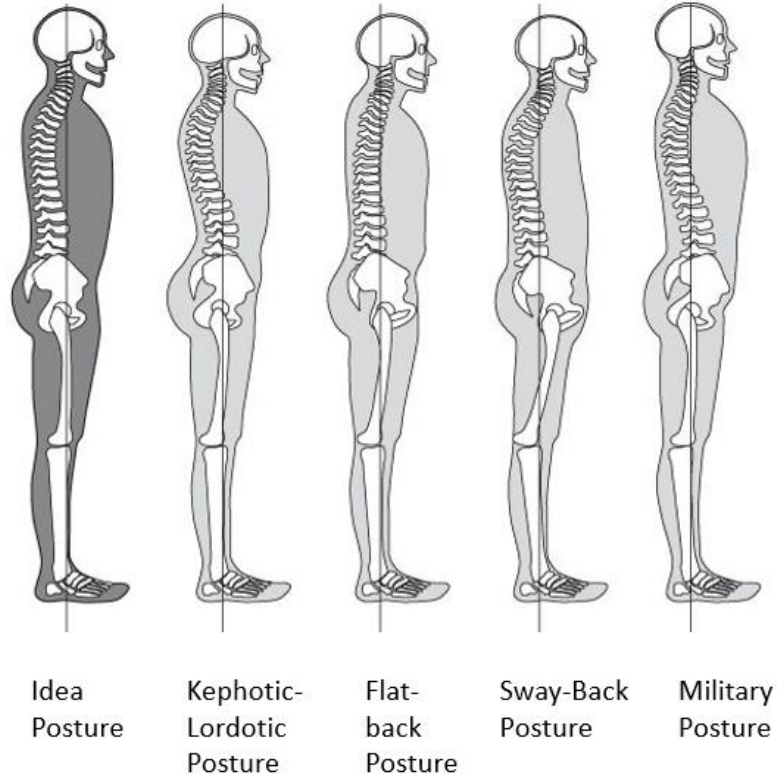


Figure 36. Body postures.

The idea posture image will firstly be resized to match the length of the human, we assume the tester is 1700mm height. The curvature of the body spine will then be extract from the idea posture image by finding the first non-zero values along the  $y$  direction for each  $x$  value shown in Figure 37. The spine curvature will be used as the deformation  $\Delta h_x$  for decide the voxel size.

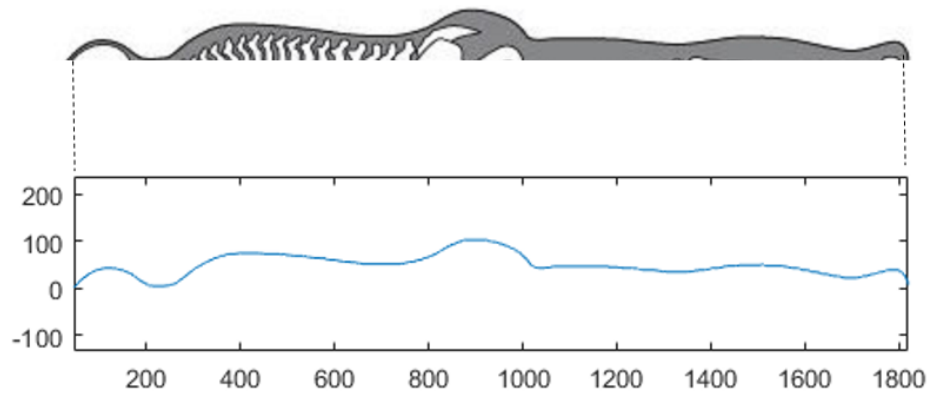


Figure 37. Idea body curvature.

Equation 7 will be simplified as Equation 20 with given  $h = 200, C_2 = 0.5323, l = 20$ .

$$t = \frac{Fh}{3l\Delta h C_2} = 6.262 \frac{F}{\Delta h} \quad (20)$$

Using Equation 10 to find the bounding box parameter  $l_x$  and  $l_y$ , calculate the mean load values  $\overline{F_{i,j}}$  of all the pixels  $x = k \dots k = m_1, y = g \dots g + n_1$  that falls in this bounding box as shown in Equation 21.

$$\overline{F_{i,j}} = \frac{1}{m_1 n_1} \sum_k^{k+m_1} \sum_g^{g+n_1} F_{x,y} \quad (21)$$

Equation 20 and 21 will give the t values for each bounding box and using Equation 11 to find the inner voxel parameters  $l_{ix}$  and  $l_{iy}$ . This process is also done in MATLAB to give all the voxel information as shown in Figure 38.

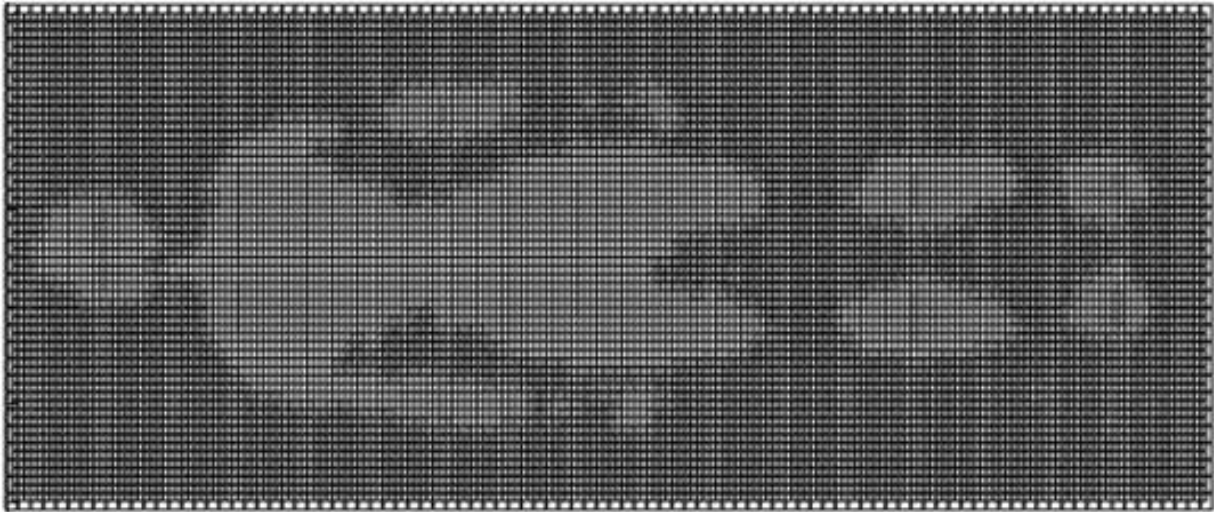
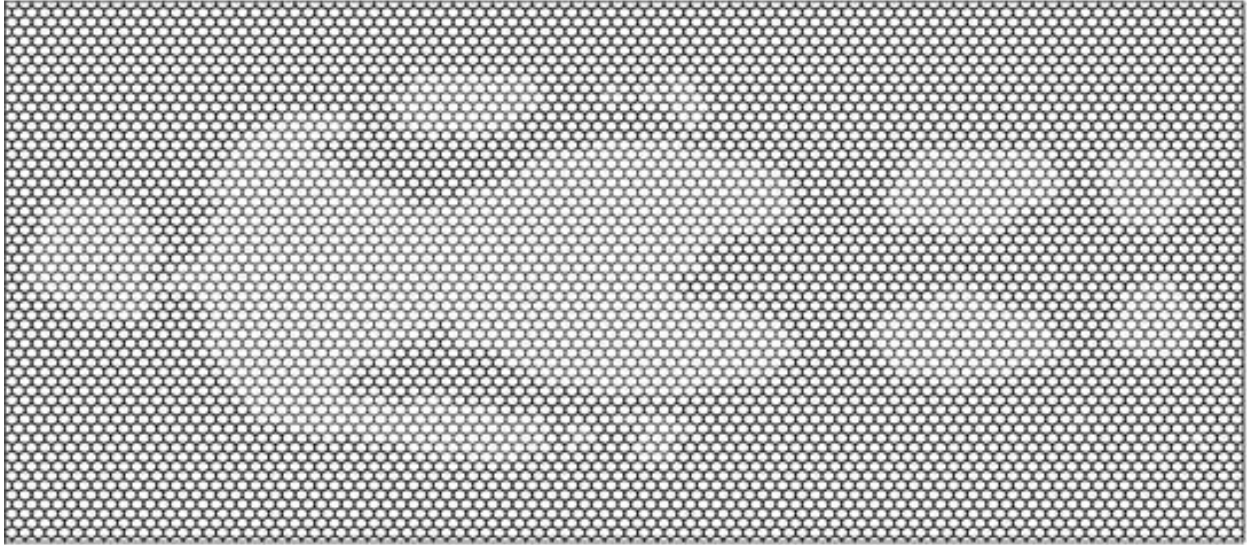


Figure 38. Voxelization of the proposed design of mattress.

Use Equation 11 to filling the voxels will give the final design as shown in Figure 39.



*Figure 39.* Fitting variable hexagons into voxels.

## **5.2. Evaluation**

The comparison between the proposed designed mattresses with a current existing mattress is done here to evaluate the proposed design, as described in 5.1, the assessment of sleep system is the spinal alignment. A uniform hexagonal mattress is modeled and calculated to find the deformation curve.

The material, cell height, and edge length will keep same as the proposed design which are  $h = 200, C_2 = 0.5323, l = 20 ; t = 2$  will be applied here to obtain uniform thickness. The final model is shown in Figure 40.

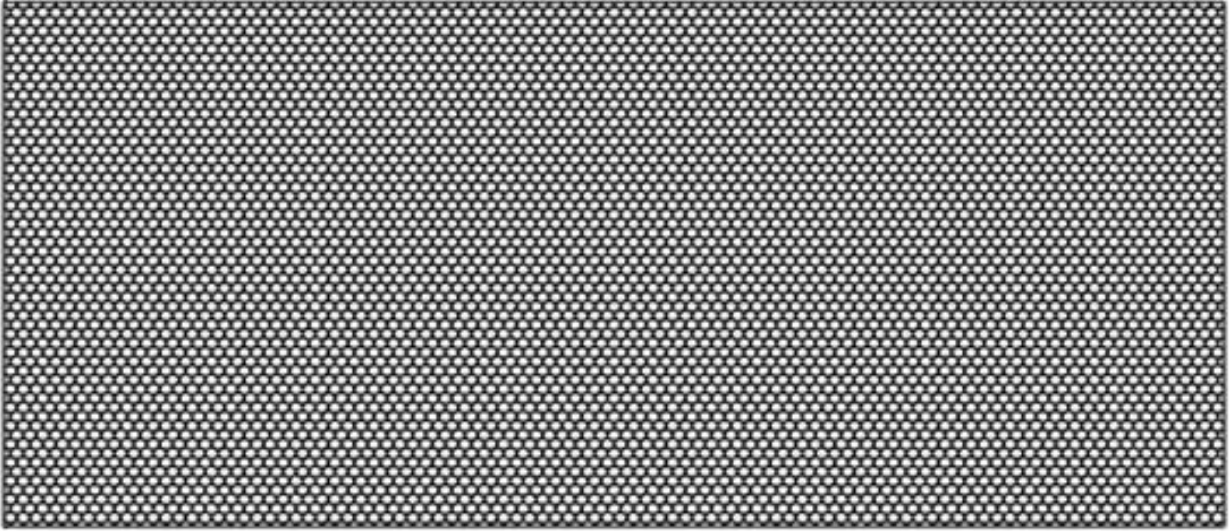


Figure 40. Model of uniform hexagonal mattress.

After getting the model, the array of deformation are found using Equation 22. And the deformation at x is the max deformation for the column. The deformation is then plot (red curve) and compared with the body curvature (blue curve) in Figure 41.

$$\Delta h_{x,y} = 6.262 \frac{F_{x,y}}{t} \quad (22)$$

$$\Delta h_i = \min \Delta h_{i,y} \quad (23)$$

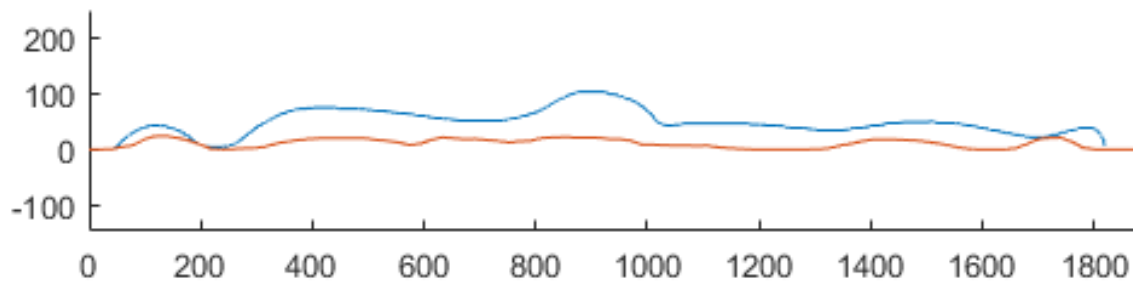


Figure 41. Comparison of the deformation between two designs.

The plot can easily tell that the proposed design will better match the body spinal curve which can better recuperate out body during sleep. However the uniform mattress will have higher possibility causing pressure ulcers.



## **6. CONCLUSION AND FUTURE DIRECTION**

### **6.1. Conclusion**

In this thesis, design and manufacturing approaches of variable stiffness cellular structure has been developed. An implementation of ergonomic mattress design has been evaluated by comparing to the existing mattress. In this study, an image analysis technique was used to extract performance information from the performance distribution map. And study of relationship between the cell parameters and performance were also given by designing, manufacturing and mechanical testing on samples. Voxelization was applied for determine the cell size and unit cells were then fitted into the voxels respectively.

The methodology can be applied to design seat cushion, shoe sole and other similar deformation-driven applications. It can also be widely used into aerospace applications since weight of the structure is reduced but the mechanical properties are maintained compare to solid objects. Also, the highlight of the methodology is to create stochastic-performance cellular structure which optimized the mechanical performance of the structure.

In conclusion, a topology design of variable performance cellular structure is achieved to enhance the performance and material efficiency. This makes the topology optimization become an effective approach on enhance cellular structures behaviors.

### **6.2. Future Direction**

Of course, there are several directions that the study can be expended, below are some of my suggestions for future research:

The relationship between performance and cell parameters can be further studied by analyze more than one parameter. Take the cuboid as example, only cell width  $w$  is studied in this research, however, by changing more than one parameter (e.g. both cell length and cell width) at

a time, not only the parameter themselves, but also the correlation between them need to be considered. At the same time, a better Gibson-Ashby model can be fitted by changing the exponents with extensive experiments done with FEA.

Performance does not limits to the elastic behavior under load but other properties. As mentioned in Chapter 1, cellular structures has multi-functionality including low weight, energy absorption and heat transfer. Design of mattress can be further improved by considering both the spine alignment and heat transfer. In order to do that, I would recommend to assign optimized weightage for both properties when determine the unit cell parameters.

Only supine sleeping posture is studied in this research because this posture introduced least intradiscal pressure when sleeping. However, considering different sleep posture in the design of mattress can reduce the discomfort. In order to do that, study of customer's sleeping habit is requirement. The required deformation at each location for all possible postures needs to be figures out by modeling the 3D body shape. Then taking into account the amount of time spent in each postures as a design factor in the analysis of spine alignment.

## REFERENCES

- Ahmadi, S. M., Yavari, S. A., Wauthle, R., Pouran, B., Schrooten, J., Weinans, H., & Zadpoor, A. A. (2015). Additively manufactured open-cell porous biomaterials made from six different space-filling unit cells: The mechanical and morphological properties. *Materials*, *8*(4), 1871-1896.
- Ahsan, A. N., Xie, R., & Khoda, B. (2017). Direct Bio-printing with Heterogeneous Topology Design. *Procedia Manufacturing*, *10*, 945-956.
- Ajdari, A., Nayeb-Hashemi, H., & Vaziri, A. (2011). Dynamic crushing and energy absorption of regular, irregular and functionally graded cellular structures. *International Journal of Solids and Structures*, *48*(3), 506-516.
- Banhart, J. (2001). Manufacture, characterisation and application of cellular metals and metal foams. *Progress in materials Science*, *46*(6), 559-632.
- Bauer, J., Hengsbach, S., Tesari, I., Schwaiger, R., & Kraft, O. (2014). High-strength cellular ceramic composites with 3D microarchitecture. *Proceedings of the National Academy of Sciences*, *111*(7), 2453-2458.
- Bitzer, T. (2012). *Honeycomb technology: materials, design, manufacturing, applications and testing*: Springer Science & Business Media.
- Chen, M., Zhu, X., Lei, H., Chen, H., & Fang, D. (2015). Effect of defect on the compressive response of sandwich structures with carbon fiber pyramidal truss cores. *International Journal of Applied Mechanics*, *7*(01), 1550004.
- Deshpande, V., & Fleck, N. (2001). Collapse of truss core sandwich beams in 3-point bending. *International Journal of Solids and Structures*, *38*(36), 6275-6305.
- Dong, L., Deshpande, V., & Wadley, H. (2015). Mechanical response of Ti-6Al-4V octet-truss lattice structures. *International Journal of Solids and Structures*, *60*, 107-124.
- Dong, L., & Wadley, H. (2016). Shear response of carbon fiber composite octet-truss lattice structures. *Composites Part A: Applied Science and Manufacturing*, *81*, 182-192.
- Evans, A. G., Hutchinson, J. W., Fleck, N. A., Ashby, M., & Wadley, H. (2001). The topological design of multifunctional cellular metals. *Progress in Materials Science*, *46*(3), 309-327.
- Fan, H., Meng, F., & Yang, W. (2007). Sandwich panels with Kagome lattice cores reinforced by carbon fibers. *Composite structures*, *81*(4), 533-539.
- Fan, H., Yang, L., Sun, F., & Fang, D. (2013). Compression and bending performances of carbon fiber reinforced lattice-core sandwich composites. *Composites Part A: Applied Science and Manufacturing*, *52*, 118-125.

- George, T., Deshpande, V. S., & Wadley, H. N. (2013). Mechanical response of carbon fiber composite sandwich panels with pyramidal truss cores. *Composites Part A: Applied Science and Manufacturing*, 47, 31-40.
- Gibson, I., Rosen, D. W., & Stucker, B. (2010). *Additive manufacturing technologies* (Vol. 238): Springer.
- Gibson, L. J., & Ashby, M. F. (1999). *Cellular solids: structure and properties*: Cambridge university press.
- Grediac, M. (1993). A finite element study of the transverse shear in honeycomb cores. *International journal of solids and structures*, 30(13), 1777-1788.
- Haex, B. (2004). *Back and bed: ergonomic aspects of sleeping*: CRC press.
- Harte, A.-M., Fleck, N., & Ashby, M. (1999). Fatigue failure of an open cell and a closed cell aluminium alloy foam. *Acta materialia*, 47(8), 2511-2524.
- Harte, A.-M., Fleck, N. A., & Ashby, M. F. (2000). Sandwich panel design using aluminum alloy foam. *Advanced Engineering Materials(Germany)*, 2(4), 219-222.
- Hollister, S. J. (2005). Porous scaffold design for tissue engineering. *Nature materials*, 4(7), 518-524.
- Hu, Y., Li, W., An, X., & Fan, H. (2016). Fabrication and mechanical behaviors of corrugated lattice truss composite sandwich panels. *Composites Science and Technology*, 125, 114-122.
- Jiang, S., Sun, F., Zhang, X., & Fan, H. (2017). Interlocking orthogrid: An efficient way to construct lightweight lattice-core sandwich composite structure. *Composite Structures*, 176, 55-71.
- Kelsey, S., Gellatly, R., & Clark, B. (1958). The shear modulus of foil honeycomb cores: A theoretical and experimental investigation on cores used in sandwich construction. *Aircraft Engineering and Aerospace Technology*, 30(10), 294-302.
- Kooistra, G. W., & Wadley, H. N. (2007). Lattice truss structures from expanded metal sheet. *Materials & Design*, 28(2), 507-514.
- Kruth, J.-P., Leu, M.-C., & Nakagawa, T. (1998). Progress in additive manufacturing and rapid prototyping. *CIRP Annals-Manufacturing Technology*, 47(2), 525-540.
- Lu, T., & Chen, C. (1999). Thermal transport and fire retardance properties of cellular aluminium alloys. *Acta Materialia*, 47(5), 1469-1485.
- Maloney, K. J., Roper, C. S., Jacobsen, A. J., Carter, W. B., Valdevit, L., & Schaedler, T. A. (2013). Microlattices as architected thin films: Analysis of mechanical properties and high strain elastic recovery. *APL Materials*, 1(2), 022106.

- Maskery, I., Hussey, A., Panesar, A., Aremu, A., Tuck, C., Ashcroft, I., & Hague, R. (2017). An investigation into reinforced and functionally graded lattice structures. *Journal of Cellular Plastics*, 53(2), 151-165.
- Nachemson, A., & Elfstrom, G. (1970). Intravital dynamic pressure measurements in lumbar discs. *Scand J Rehabil Med*, 2(suppl 1), 1-40.
- Nonell, J. B. (2000). *Antonio Gaudi: master architect*: Abbeville Press.
- Piegl, L., & Tiller, W. (1995). *The NURBS Book*, Springer-Verlag. *New York*.
- Pressure Imaging for Mattress Design. (2013). Retrieved from <https://www.tekscan.com/applications/pressure-imaging-mattress-design>
- Shipbuilding, R. S. PO Box, 16 4380 AA Vlissingen. *The Netherlands*.
- Triantafyllidis, N., & Schraad, M. (1998). Onset of failure in aluminum honeycombs under general in-plane loading. *Journal of the Mechanics and Physics of Solids*, 46(6), 1089-1124.
- Valdevit, L., Pantano, A., Stone, H. A., & Evans, A. G. (2006). Optimal active cooling performance of metallic sandwich panels with prismatic cores. *International Journal of Heat and Mass Transfer*, 49(21), 3819-3830.
- Wadley, H. N. (2006). Multifunctional periodic cellular metals. *Philosophical Transactions of the Royal Society of London A: Mathematical, Physical and Engineering Sciences*, 364(1838), 31-68.
- Wang, A.-J., & McDowell, D. (2004). In-plane stiffness and yield strength of periodic metal honeycombs. *Journal of engineering materials and technology*, 126(2), 137-156.
- Xiong, J., Ma, L., Pan, S., Wu, L., Papadopoulos, J., & Vaziri, A. (2012). Shear and bending performance of carbon fiber composite sandwich panels with pyramidal truss cores. *Acta Materialia*, 60(4), 1455-1466.
- Xiong, J., Ma, L., Wu, L., Wang, B., & Vaziri, A. (2010). Fabrication and crushing behavior of low density carbon fiber composite pyramidal truss structures. *Composite Structures*, 92(11), 2695-2702.
- Zok, F. W., Waltner, S. A., Wei, Z., Rathbun, H. J., McMeeking, R. M., & Evans, A. G. (2004). A protocol for characterizing the structural performance of metallic sandwich panels: application to pyramidal truss cores. *International Journal of Solids and Structures*, 41(22), 6249-6271.